UNIVERSITÀ DEGLI STUDI DI NAPOLI FEDERICO II

SCHOOL OF MATHEMATICS, PHYSICS AND NATURAL SCIENCES

PHD IN CHEMICAL SCIENCES, CYCLE XXVIII

Computational and structural study of model and industrial Ziegler-Natta catalysts

Emanuele Breuza

SUPERVISOR

PROF. VINCENZO BUSICO

ASSESSOR

PROF. GIOVANNI TALARICO

COORDINATOR

PROF. LUIGI PADUANO

To my Father that with great passion and a lot of patience

thought me how beautiful (and sometimes painful)

a human life could be…

Table of contents

Acknowledgments

This work is part of the research program of the Dutch Polymer Institute (DPI), project #754.

We acknowledge the CINECA and the Regione Lombardia award under the LISA initiative, for the availability of high performance computing resources and support.

Chapter 1. Introduction to Ziegler-Natta catalysis for isotactic polypropylene

1.1 Overview

With an annual production that has more than doubled over the last 10 years (to 55.1 million metric tons in 2013, corresponding to a revenue of ~$65 billion), isotactic polypropylene (iPP) is the second largest volume polymer on the market. It alone accounts for approximately 2.5% of the overall chemical sales per year. Revenues are expected to increase to >$100 billion by 2021.[1] Introduced more than 50 years ago, Ziegler–Natta catalysts (ZNC) have a dominant position in the industrial production of iPP. The original ZNC were simply some form of $TiCl_3$ activated by aluminum alkyls,[2] and were characterized by low activity and low stereoselectivity.[3] Gradual improvement has led to much more efficient and selective catalysts containing Ti centers on a $MgCl_2$ support.[3-4] The formulation of these catalysts involves recipes developed in a mostly empirical fashion. The following is a general description of just one of the many procedures for creating such a catalyst:[3]

- Ball-milling of $MgCl_2$ with $TiCl_4$ and a small amount of a Lewis base (called the Internal Donor, ID);
- Removing the excess of $TiCl_4$ by washing;
- Activation with excess of trialkylaluminum (R_3Al) and a second Lewis base (called the External Donor, ED).

Rational catalyst design/development has been a long-standing challenge, seriously hampered by a lack of fundamental knowledge of the precise roles of the various catalyst components. The multisite nature and the low concentration of active sites make traditional experimental surface science methodologies towards active site characterization difficult.[5] And despite continuing growth of the iPP market, both industry and academia appear to be reducing investments in fundamental studies of these catalysts, perhaps considering them too "mature".[6] However, in reality ZNC will not become truly mature until they are understood much better than they currently are.

In view of the problems facing surface science characterization methods, it seems logical that computational methods will have to play an important role in addressing questions not amenable to experimental verification,[7] such as the roles of the various catalyst components of ZNC, the bonding mode and location of Ti species on $MgCl_2$ particles, and the precise coordination environment around the various active Ti sites in activated catalysts. Due to developments in computational codes and hardware over the last decade, realistic models of active sites are coming within reach of modern DFT methods.[8] In this thesis we present an approach towards the construction of reasonably complete chemical models of ZNC, starting from $MgCl_2$ clusters, determining where and how internal donors and $TiCl_4$ adsorb, and ending with ternary systems containing both Ti and donors bound in each other's vicinity on $MgCl_2$. This allows us to evaluate the validity of a number of widely held, but never

rigorously tested, assumptions regarding adsorption sites, binding strength, and roles of Ti species and donors.

1.2 Introduction to Ziegler-Natta Catalysts

1.2.1 From $TiCl_3$ to $Ti/MgCl_2$

Present-day ZNCs for iPP are a direct derivation of those discovered in the laboratories of Giulio Natta at the Milan Polytechnic in 1954, featuring $TiCl_3$ in one of its 'violet' crystalline modifications with a layer structure (α, γ, δ) as the solid pre-catalyst.[2] Detailed investigation of the polymorphism of $TiCl_3$ has highlighted that the chirality of the Ti centers in the octahedral cavities of the structural layers is maintained on the crystal edges (**Figure 1.1**).[9] Thus, the much higher stereoselectivity in propene polymerization of these modifications, compared with the 'brown' polymorph with fibrillar structure and non-chiral Ti originally obtained by Ziegler, found an immediate and convincing explanation.[10] In the following years this concept was probably over-emphasized, which may ultimately have slowed the understanding of later catalyst generations with much smaller primary particles.

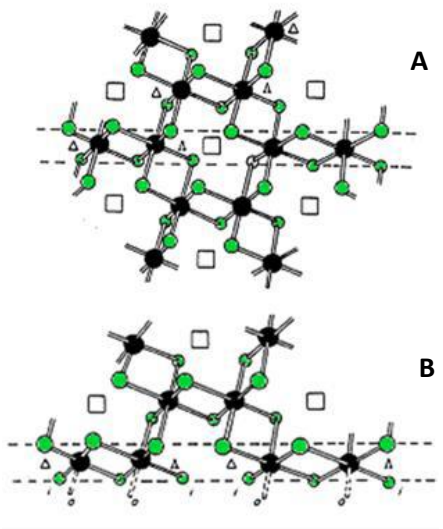

Figure 1.1 Schematic representation of a 'violet' $TiCl_3$ structural layer, before (**A**) and after (**B**) being cut along the (110) crystallographic direction. The Δ or Λ chirality of the Ti centers is explicitly indicated.[9]

The main drawback of $TiCl_3$-based catalysts was the low yield, resulting into non-negligible residual amounts of acidic Ti-Cl bonds in the polymer, which had to be subjected to intensive processes of catalyst deashing.[3-4] Supporting the active Ti species on an inert matrix, thus increasing the productivity per Ti, looked like an obvious solution to the problem. However, the bulk of the crystal in 'violet' $TiCl_3$ is not an innocent self-support, because its structure determines the stereogenic environment of the exposed Ti centers. As a matter of fact, when typical supports like calcined silica or alumina were impregnated with $TiCl_4$ and reacted with R_3Al for Ti alkylation/reduction, the results were very poor (at most moderate activity in the polymerization of ethene, low or no activity and no stereoselectivity in propene polymerization).[3-4] Much better performances were achieved using a MgO "support". It did not take too

long to realize that $TiCl_4$ chlorinates MgO, ending up with $MgCl_2/TiCl_4$ adducts. The halogenated salt has a crystalline structure very similar to that of 'violet' $TiCl_3$; indeed Cl-Mg-Cl 'sandwiches'[3-4] are stacked in consecutive layers in which all octahedral cavities in between the two Cl planes are occupied by Mg (as opposed to Ti in 2/3 of the cavities in $TiCl_3$).[10] Using authentic $MgCl_2$ as support led to even better catalysts for polyethylene. Performance for polypropylene was less satisfactory: productivity increased to over 150 kg of polymer per gram of Ti, but less than 40% of the product was 'isotactic'. However, the addition of proper Lewis bases (LB) to the formulation, as components of the solid pre-catalyst or complexed with the R_3Al, improved both the productivity (up to 2 tons of polymer per gram of Ti) and the stereoselectivity (>95% 'isotactic' polymer).[3-4]

The aforementioned similarity in crystal structure between $MgCl_2$ and 'violet' $TiCl_3$ suggested extension of the crystallochemical approach used by Cossee and Arlman[11] for $TiCl_3$ to these new $MgCl_2$ supported pre-catalysts. The starting assumption was that $TiCl_4$ chemisorption can only take place at coordinatively unsaturated faces of $MgCl_2$ crystals. According to Giannini[12] and Corradini,[13] the most plausible layer terminations of $MgCl_2$ are (104)* and (110), respectively exposing 5 and 4-coordinated Mg atoms. A pioneering paper by Corradini and co-workers[13] proposed that

* The "(100)" edge mentioned by Corradini is more appropriately called (104); we will use the (104) notation in the remainder of this thesis even where original authors used "(100)".[[[ref]]]

stereoselective active species would result from the epitaxial chemisorption of dinuclear Ti_2Cl_8 adducts on (104) surfaces, followed by alkylation and reduction by R_3Al (see **Figure 1.2-A** and **A**^{I}). Indeed, the close similarity in the local coordination environment of Ti between this model and authentic edges of 'violet' $TiCl_3$ is certainly impressive. On the other hand, sterically more open (albeit chiral) non-stereoselective active species could form by mononuclear epitaxial $TiCl_4$ chemisorption on (110) lateral terminations (**Figure 1.2-B** and **B**^{I}). This undesired case was postulated to be largely prevented by the addition of a suitable ID, which would bind to the highly Lewis-acidic 4-coordinated Mg atoms more strongly than $TiCl_4$.[13] Years later, one particular class of ID (1,3-dimethoxypropanes) was actually claimed to have been specifically designed based on this model: it was expected to chelate preferentially to 4-coordinate Mg on (110) edges.[14]

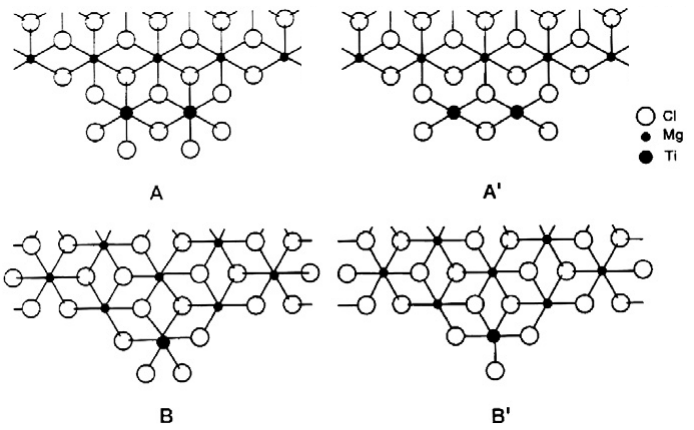

Figure 1.2 Epitaxial models of Ti_xCl_{4x} (**A** and **B**) and Ti_xCl_{3x} (**A**^{I} and **B**^{I}) species on lateral $MgCl_2$ crystal terminations, according to Corradini et al.[13]

1.2.2 ZNC synthesis

The preparation procedure of ZNC precursors consists of several steps that result in the formation of $MgCl_2$ nano-particles on which are chemisorbed $TiCl_4$ (source of catalytically active metal) and a Lewis base (the internal donor, ID). Finally, the catalyst is activated by addition of trialkylaluminum (R_3Al) mixed with a second Lewis base (the external donor, ED).[3] This mixture of ingredients results in a large number of species that interact each other, and the final catalyst behavior depends in a sensitive way on the balance between these interactions.

As mentioned earlier, one way to prepare the pre-catalyst is intensively milling $MgCl_2$, $TiCl_4$ and ID, or $MgCl_2$ and ID alone followed by impregnation of the solid with neat or concentrated $TiCl_4$ at high temperature (titanation reaction). Subsequently, excess of $TiCl_4$ and ID is removed by hot-washing with hydrocarbons.[15] Pre-catalysts prepared in this way typically contain 1 ÷ 2 wt-% of Ti and 5 ÷ 10 wt-% of ID. The commonly accepted interpretation of this protocol is that $TiCl_4$ adsorbs strongly on certain sites of the $MgCl_2$ surface, stabilized and possibly modulated by the ID, and then remains firmly bound during subsequent washing, activation and catalysis. The drawback of this preparation is that it does not allow much control over the shape of the initial catalyst particles. Since this shape will be replicated later on by the shape of the iPP particles produced, the lack of morphology control results in a polymer less suitable for future manipulations. More recent preparation routes start from soluble or low-melting $MgCl_2$ precursors (e.g. MgR_2, or $MgCl_2$/alcohol

adducts).[16] With the aid of emulsion, spray-drying or spray-cooling technologies, the organic phase is removed. Reaction with excess $TiCl_4$ at high temperature in the presence of the ID then leads to pre-catalyst secondary particles featuring high porosity and well-controlled spherical morphology. These are aggregates of billions of primary $MgCl_2$/$TiCl_4$/ID nano-particles of smaller size, with higher Ti and ID contents (up to 5 wt-% and 20 wt-%, respectively), but structurally similar to those obtained by physical methods.

It is generally believed that $MgCl_2$ acts as an inert carrier for $TiCl_4$, from which the catalytic species form by reaction with the R_3Al activator via alkylation and reduction, mainly to the Ti(III) oxidation state.[3] Moreover, the trialkylaluminum activator has the additional and crucial role of scavenger of ubiquitous impurities (primarily heteroatom-containing molecules like water and oxygen, lethal to the highly oxophilic Ti species).[3] Also other functions (such as a direct interaction with the active Ti species) have been proposed based on the massive adsorption of Al-containing species on the solid phase, but these suggestions have not found much support.

The role of the ID during pre-catalyst synthesis is to stabilize support primary particles by chemisorption onto unsaturated Mg sites, thus lowering surface energy of lateral terminations and promoting the formation of a compact matrix with high specific surface area.[17] In addition, it is widely accepted that LB molecules (both ID and ED) co-adsorbed in the vicinity of inherently chiral but relatively open surface Ti species provide

the necessary hindrance for the transition metal centers to effectively discriminate between the two enantiofaces of the prochiral propene molecules at the insertion step.[18] This role is undeniable and crucial, as is demonstrated by the fact that practically all aspects of the catalytic performance depend on the specific nature of the LBs present in the system (**Table 1.1**). This being said, it is worth recalling here that all ZNCs are 'multi-sited', featuring multiple classes of active species that differ –inter alia – in selectivity and molar mass capability. As far as the former aspect is concerned, even the best industrial systems contain some active species yielding small amounts of PP of comparatively low stereoregularity. The relative amount of this byproduct can be quantified by means of solvent fractionation (e.g. dissolution in hot xylene followed by fractional precipitation, or extraction by boiling heptane); the percentage by weight of the insoluble 'isotactic' PP fraction is usually defined 'Index of Isotacticity' (II), and is dramatically enhanced by proper ID/ED combinations. LBs also affect the PP molar mass, shifting it to higher average values and modulating its distribution, depending again on the specific ID/ED pair used (see M_w/M_n column in **Table 1.1**).

Table 1.1 Typical formulations and performance of ZNCs for iPP.

Internal Donor (ID)	External Donor (ED)	Productiviry [10^3 Kg(PP)/g(Ti)]	Index of Isotacticity, II	M_w/M_n
ethyl benzoate	methyl *p*-toluate	0.5	>95	5 ÷ 7
dibutyl phthalate	$R^1R^2Si(OMe)_2$	1 ÷ 2	>97	5 ÷ 7
2,2-dialkyl-1,3-dimethoxypropane	$R^1R^2Si(OMe)_2$ (optional)	>2	>97	3 ÷ 5
dialkyl succinate	$R^1R^2Si(OMe)_2$	1 ÷ 2	>98	>7

1.2.3 Surface science and spectroscopic studies

The number of direct experimental observations of ZN pre-catalysts is limited. These solids are extremely reactive, so even the smallest amounts of poisoning agents could alter the sample and consequently affect the results.

Based on High-Resolution TEM images (**Figure 1.3**), Terano[19] reported that 'activated' $MgCl_2$ samples exhibit, in addition to the basal (001) planes, two kinds of lateral terminations, namely 'atomically flat' (assumed to belong to (110)-type surfaces) and 'atomically rough' planes (perpendicular to the former). The adsorption of $TiCl_4$ on $MgCl_2$ severely distorts the crystals and makes their surfaces 'no longer atomically flat planes'.[19]

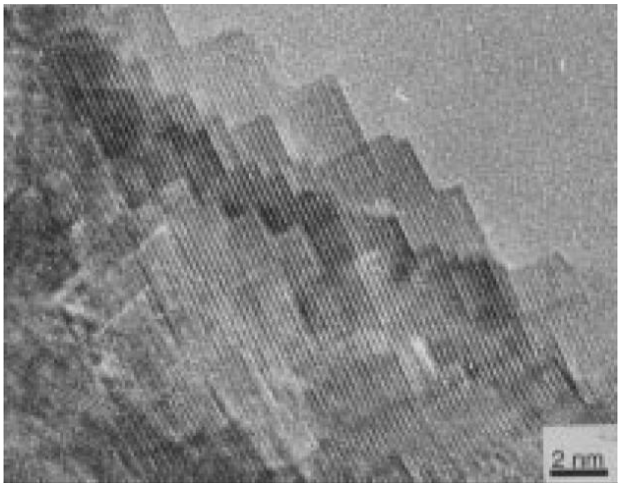

Figure 1.3 High Resolution TEM image of an 'activated' crystalline $MgCl_2$ sample.[19]

Electron Microscopy observations carried out by Oleshko[20] and Thüne[21] demonstrated that samples obtained from $MgCl_2 \bullet n$ROH precursors contain crystalline domains along with regions characterized by extensive

disorder[22] (**Figure 1.4**). This seems to confirm that, in spite of differences in morphology, the structures of physically and chemically activated ZNCs are basically the same.

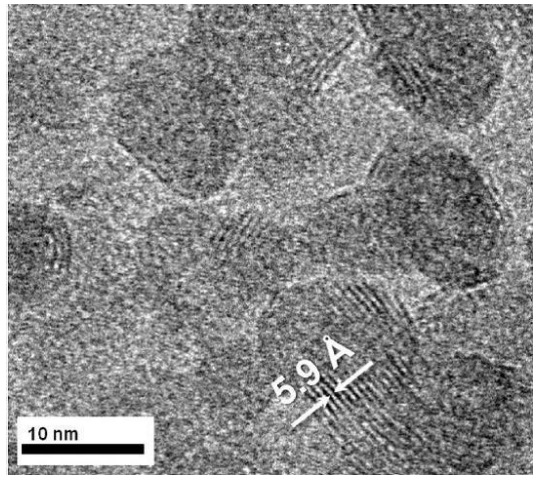

Figure 1.4 TEM image of $MgCl_2$ film spin-coated from an EtOH solution at 30°C. The highlighted spacing of 5.9 Å is typical of the layer structure of crystalline $MgCl_2$.[40]

Studies of active Ti sites are even more challenging since these species represent only a small fraction of the total amount of Ti present. Magni and Somorjai[23] studied the interaction of $TiCl_4$ with $MgCl_2$ films grown on a gold support. They found that at low temperature (<110 K) $TiCl_4$ binds only weakly and it is completely removed on evacuation. On the other hand, much more strongly bound species are obtained when a high temperature (~300 K) is applied before evacuating; indeed, heating up to the sublimation temperature of $MgCl_2$ is then required to remove the residual adsorbate molecules. The amount of this $TiCl_4$ corresponds roughly to 1 ÷ 2 wt-% of Ti, i.e. close to that found in actual pre-catalysts. The authors described the strongly bound species as being incorporated into

the 'bulk' of $MgCl_2$, without going into details or discussing the implications for catalysis. Recent vibrational spectroscopic studies by Zerbi[15g, 24] concluded that surface Ti species in ZNCs are most likely octahedral $TiCl_4$ units bound to 4-coordinated Mg (e.g., on $MgCl_2$(110) or equivalent surfaces). While both of these studies provide some information about the majority Ti species on the support, it cannot be simply assumed that the results also apply to the actual active Ti sites.

1.3 Modelling of Ziegler-Natta Catalysts

1.3.1 From Molecular Mechanics to Quantum Mechanics

Until the late 1980s, Molecular Mechanic (MM) was the only available computational tool capable of simulating ZNC systems.[9, 25] This technique is based on empirical parametrization of interactions between the atoms of the systems simulated, with the presence or absence of bonds decided by the researcher. The quality of the results is mainly determined by the quality of the parametrization. High-quality parametrizations are available for organic molecules but not for metal atoms. In addition, MM methods do not handle making and breaking of chemical bonds, thus precluding prediction of reaction barriers. Some very interesting results have been obtained based on judicious use of MM, as illustrated by Corradini's 'growing chain orientation mechanism of stereocontrol' that still remains a milestone in the development of understanding of stereoselective olefin polymerization.[26] Nevertheless,

nowadays MM has been mostly superseded by the use of electronic structure methods, at least for systems smaller than proteins.

This being said, it is also important to realize that a *rigorous* Quantum Mechanical (QM) treatment is still unfeasible at present for systems with more than 20 atoms, and therefore approximations like Density Functional Theory (DFT) are required. Current DFT methods work well with systems featuring localized bonds, but have significant shortcomings in describing medium and long-range interactions, which is important in describing crystal structures (e.g. the inter-layer interactions in $MgCl_2$) as well as weak coordination complexes (e.g. olefin complexation).[27] A few benchmark papers[27-28] published recently indicate that the large majority of DFT functionals, whether based on Local Density Approximation (LDA), Generalized Gradient Approximation (GGA) or even the most popular meta-GGA, do not describe models relevant to ZNC systems well (compared to Coupled Cluster calculations as reference). Indeed, standard DFT methods do not adequately reproduce dispersion forces, and whenever such interactions are non-negligible, semi-empirical ad-hoc corrections must be introduced in the calculations (see next section for details). Very recently, new generations of functionals covering medium and long-range correlations have been implemented, some specifically for use with crystals, and these seem to perform rather well,[27] but their adoption is not yet widespread. Despite its shortcomings, DFT (with suitable choices of functional and dispersion corrections) is currently the only practical method for studying catalytic systems like ZNC.

Given the choice for DFT and a particular functional, another important issue is the selection of basis sets. The first requirement is that basis sets for different elements in a molecule are balanced, else completely unrealistic electronic structures can be obtained. In addition, special precautions may be needed for specific situations, such as the addition of diffuse functions for atoms with a large negative charge (e.g. Cl).[27] Unfortunately, in the last 20 years many DFT studies of ZNCs have been published without a serious analysis of the aforementioned aspects, which means that their results are potentially flawed.

1.3.2 Dispersion corrected DFT Modelling

Dispersion forces are all non-covalent interactions between two different molecules (or molecules and the surface of a solid material) left after electrostatic (ion-dipole, dipole-dipole,...) interactions have been accounted for. These interactions, also called Van der Waals or London forces, play an important role in physisorption as well as chemisorption phenomena. The vast majority of DFT functionals do not describe such long-range interactions well.

Recently, new DFT functionals (the M05 and M06 families)[29] were developed in order to describe both short and long range interactions as well as transition-metal bonding with high accuracy. These methods were constructed by a systematic fitting of experimental and computational data. Due to the large number of parameters and the complexity of the equations adopted, such functionals are more time-demanding, which may be a problem for investigation of very large systems.

The solution proposed by Grimme and coworkers,[30] on the other hand, combines accuracy and efficiency (but possibly with a more limited range of validity). Indeed it can be used with any DFT functional as well as for HF calculations, although different parametrizations may be required for different functionals. The authors define the dispersion-corrected total energy E_{MF-D} as follow:

$$E_{MF-D} = E_{MF} + E_{disp} \qquad \textbf{Eq. 1.1}$$

where E_{MF} is the mean-field energy (i.e. calculated using HF or a DFT method) and E_{disp} is an empirical dispersion correction. They then expand E_{disp} in a series of R_{ij}^{-6} terms (i.e. the distance between two atoms to the power of -6) using atom-pair dispersion coefficients C_6^{ij} estimated from per-element coefficients ($C_6^{ij} = \sqrt{C_6^{ii} C_6^{jj}}$):

$$E_{disp} = -s_6 \sum_{i=1}^{N-1} \sum_{j=i+1}^{N} \frac{C_6^{ij}}{R_{ij}^6} f_{dmp}(R_{ij}). \qquad \textbf{Eq. 1.2}$$

Here, s_6 is a global scaling factor that depends on the functional applied to calculate the mean-field energy and N is the number of atoms in the system. To avoid overestimation of the correction between atoms with a distance well below typical Van der Waals radii (mostly bonded atoms), a damping function f_{dmp} is applied:

$$f_{dmp}(R_{ij}) = \frac{1}{1 + e^{-\alpha(R_{ij}/R_{ij}^0 - 1)}} \qquad \textbf{Eq. 1.3}$$

α is a constant value that determines the steepness of the damping function and R_{ij}^{0} is the sum of atomic Van der Waals radii. This function decays very rapidly for small R_{ij}, resulting in a negligible contribution of dispersion corrections between bonded atoms.

1.3.3 Periodic DFT-D Modelling

Modelling crystal structures or perfect crystal surfaces or edges is best done using periodic calculations. Periodic QM methods are inherently more complex than isolated-molecule methods. The first periodic DFT-D studies[31] on $MgCl_2$ explicitly addressing all 'technical' aspects of the calculations came from inside the research group hosting the present thesis. Here periodic boundary conditions were adopted to investigate the relative stability of the most common surfaces exposed by a crystal of neat $MgCl_2$. Inclusion of dispersion forces was found to be beneficial for describing inter and intra-layer interactions. In particular, the authors observed that both well-formed models (in which relative surface stability determines the crystal morphology) and those ones obtained considering kinetic factors (using the method of Bravais, Friedel, Donnay and Harker)[32] should only feature basal planes and lateral terminations with 5-coordinated Mg (i.e. (104) or equivalent; **Figure 1.5**). Surfaces exposing 4-coordinated Mg (i.e. (110) or equivalent) are significantly higher in energy, and should at most constitute a small minority.

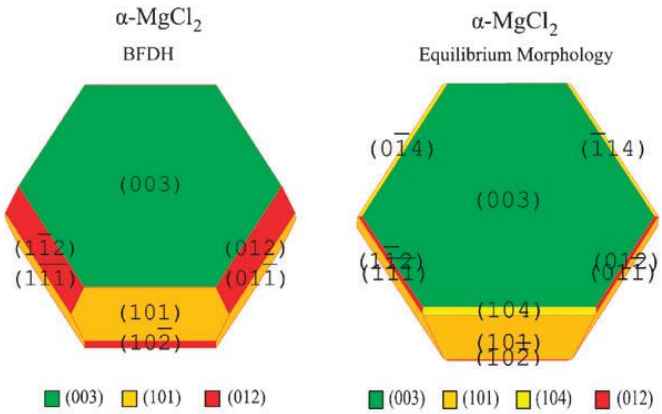

Figure 1.5 Crystal morphologies predicted for α-$MgCl_2$ using Bravais, Friedel, Donnay and Harker (BFDH)[31b] and equilibrium models.

On the other hand, a more recent paper using the same computational approach reported that the relative stability of $MgCl_2$ surfaces can be completely altered in presence of small LB molecules (i.e. H_2O, NH_3 and EtOH).[33] Indeed, the energy of formation of the (110) surface was predicted to become negative if the surface was covered in adsorbate molecules, meaning that even partially saturated (110) surfaces are more stable than $MgCl_2$ bulk. As a matter of fact, H_2O and EtOH are good solvents for this salt. Considering now the difference between adsorption energies on surfaces exposing 5 and 4-coordinated Mg, the latter turned to be favored only when a 2:1 ratio of LB to surface Mg was employed. This being said, steric repulsions seem to become already important for EtOH molecules, leading to a larger energy drop between the coordination energies of the first and second molecule (but see next section).

Perhaps the most important contribution of periodic DFT-D simulation to the ZNC field relates to the study of $TiCl_4$ chemisorption on

$MgCl_2$. This problem has been addressed by several computational groups, leading to many different and inconsistent conclusions. To analyze this unusually large disagreement, Busico and co-workers[27] performed a careful investigation of the effects of different choices of density functional and basis set, concluding that $TiCl_4$ adsorption is a 'dispersion-driven' process and therefore dispersion contributions are mandatory for a correct analysis of ZNC systems. Results indicate that $TiCl_4$ will only bind to lateral terminations exposing 4-coordinated Mg atoms, e.g. $MgCl_2$(110) or defect sites with similar properties.[34] In particular, neither monomeric nor dimeric $TiCl_4$ units appear to bind to $MgCl_2$(104).

Therefore, long-standing hypotheses[3-4, 13, 14b, 35] on the genesis of the stereoselective active species for propene polymerization and roles of added LB need to be re-considered (see **Chapter 3** and **4** for a more detailed description).

1.3.4 Periodic vs Cluster approaches

Periodic studies are extremely useful for studying crystal bulk and perfect surfaces and edges. However, they are less suited for the description of isolated species (point defects, corners, active Ti sites) on a surface or edge.[33] Due to the periodic nature of the calculation, very large unit cells are needed to isolate one "isolated species" from its neighbors. Since the cost of a periodic DFT calculation scales as $\sim V^2$ to $\sim V^3$, using very large unit cells is impractical.

Even when modelling densely adsorbed species, periodic boundary conditions may be too restrictive. Consider for example an $MgCl_2$ edge with

one EtOH molecule per exposed Mg atom. The "natural" choice of a unit cell containing exactly one EtOH molecule implicitly forces all EtOH molecules on the edge to have exactly the same conformation. An arrangement with alternating different conformations might be lower in energy but describing this requires - again - a larger cell. A more insidious issue is that need for a larger cell may never become obvious, leading to artificially low binding energies.

Finally, it is not entirely logical to use periodic calculations for the study of catalytic reactions. Catalytic events are rare and will surely not happen in periodic "lock-step" on a surface or edge. Conceptually, at least, molecular calculations (or "embedding" methods)[36] make more sense for such applications.

The alternative to periodic studies is the "cluster approach", where a chunk of crystal is used to model an active site.[8, 36-37] The cluster model needs to be large enough so that the site of interest "feels" the same environment as it would on a crystal surface/edge. The cluster representing the crystal environment needs to be properly terminated, and this is not always trivial. Sometimes artificial terminating groups or ligands can be used. Judicious use of constraints may be helpful but also introduces some degree of arbitrariness. Often, even a minimally realistic cluster model is not small.

Cluster approaches are ideal for modelling "rare" species on surfaces, or for studying single defect sites (e.g. corners or steps) typical of real nano-particles.[3, 38] They are also suitable for the study of catalytic

events. As an added advantage, advanced QM methods like continuum solvation and TD-DFT are automatically available for cluster methods but have not yet been implemented in periodic codes. However, if the cluster is small relative to the real system, the part of the model representing the crystal bulk may be unrealistically flexible and may show artificial deformations. In the particular case of $MgCl_2$, describing a chunk of a monolayer of $MgCl_2$ using a cluster model is straightforward, but modelling chunks of multiple layers is problematic for various reasons.

In the end, it appears that there is not one universally preferable method and a balanced multi-method approach is needed. Questions related to surface stability and preferential adsorption are best addressed through periodic calculations, while catalytic events are probably better studied using cluster models. And finally, questions involving isolated active sites interacting with neighboring layers would be hard to address with present-day methods.

1.4 Scope of this thesis

The present thesis describes an approach towards realistic models of active sites in ZNC. These active sites are thought to be Ti sites on edges or defects of $MgCl_2$ nano-particles. A key question here is: "How small is a ZNC primary particle?" It turns out that these nano-particles are not much larger than minimal monolayer cluster models of $MgCl_2$. Therefore, the present thesis focuses on cluster models of ZNC. For the same reason,

artificial constraints representing the perfect crystal environment were not used (for a primary particle there is not much of a "crystal environment").

Chapter 2 of this thesis addresses the issue of primary particle size and compares results for periodic and cluster calculations on $MgCl_2$ with and without adsorbed small molecules.

Chapter 3 then uses the cluster approach to study the adsorption of realistic donor molecules (e.g. mono- and diesters, 1,3-diethers, alkoxysilanes) on $MgCl_2$ edges.

Chapter 4 re-visits the adsorption of $TiCl_4$ on $MgCl_2$ clusters of different shape.

Chapter 5, finally, addresses the complex problem of ternary ($MgCl_2$/LB/$TiCl_4$) systems and the potential environments of active sites.

References

1. Ceresna Research Market Study: Polypropylene, 2014, http://www.ceresana.com/en/market-studies/plastics/polypropylene/.
2. (a) Boor, J., Jr, *Ziegler-Natta Catalysts and Polymerizations*. Academic Press: New York (NY), 1979; (b) Kissin, Y. V., *Isospecific polymerization of olefins*. 1 ed.; Springer-Verlag New York: New York, 1985; p 439.
3. Moore, E. P., Jr., Ed., *Polypropylene Handbook: Polymerization, Characterization, Properties, Processing, Applications*. Hanser Publishers: Munich, Germany: 1996.
4. Cecchin, G.; Morini, G.; Piemontesi, F., Ziegler-Natta Catalysts. In *Kirk-Othmer Encyclopedia of Chemical Technology*, John Wiley & Sons, Inc.: 2000.
5. (a) Warzelhan, V.; Burger, T. F.; Stein, D. J., *Die Makromolekulare Chemie* **1982,** *183* (2), 489-504; (b) Kissin, Y. V., *J. Catal.* **2001,** *200* (2), 232-240; (c) Barabanov, A. A.; Sukulova, V. V.; Matsko, M. A.; Zakharov, V. A., *J. Mol. Catal. A: Chem.* **2015,** *396* (0), 328-334.
6. Busico, V., *Dalton Transactions* **2009,** (41), 8794-8802.
7. Taniike, T.; Terano, M., *Macromol. Rapid Commun.* **2007,** *28* (18-19), 1918-1922.
8. Credendino, R.; Pater, J. T. M.; Correa, A.; Morini, G.; Cavallo, L., *J. Phys. Chem. C* **2011,** *115* (27), 13322-13328.
9. Corradini, P.; Barone, V.; Fusco, R.; Guerra, G., *Eur. Polym. J.* **1979,** *15* (12), 1133-1141.
10. Natta, G.; Corradini, P.; Allegra, G., *Journal of Polymer Science* **1961,** *51* (156), 399-410.
11. (a) Cossee, P., *J. Catal.* **1964,** *3* (1), 80-88; (b) Arlman, E. J.; Cossee, P., *J. Catal.* **1964,** *3* (1), 99-104; (c) Arlman, E. J., *J. Catal.* **1964,** *3* (1), 89-98.
12. Giannini, U., *Die Makromolekulare Chemie* **1981,** *5* (S19811), 216-229.
13. Corradini, P.; Barone, V.; Fusco, R.; Guerra, G., *Gazz. Chim. Ital.* **1983,** *113* (9-10), 601-7.
14. (a) Scordamaglia, R.; Barino, L., *Macromol. Theory Simul.* **1998,** *7* (4), 399-405; (b) Albizzati, E.; Giannini, U.; Morini, G.; Galimberti, M.; Barino, L.; Scordamaglia, R., *Macromol. Symp.* **1995,** *89* (1), 73-89.

15. (a) Di Noto, V.; Bresadola, S., *Macromol. Chem. Phys.* **1996,** *197* (11), 3827-3835; (b) Di Noto, V.; Fregonese, D.; Marigo, A.; Bresadola, S., *Macromol. Chem. Phys.* **1998,** *199* (4), 633-640; (c) Bart, J. C. J., *JOURNAL OF MATERIALS SCIENCE* **1993,** *28* (1), 278-284; (d) Giunchi, G.; Allegra, G., *J. Appl. Crystallogr.* **1984,** *17* (3), 172-178; (e) Kashiwa, N., *Polym. J.* **1980,** *12* (9), 6; (f) Brambilla, L.; Zerbi, G.; Nascetti, S.; Piemontesi, F.; Morini, G., *Macromol. Symp.* **2004,** *213* (1), 287-302; (g) Brambilla, L.; Zerbi, G.; Piemontesi, F.; Nascetti, S.; Morini, G., *J. Mol. Catal. A: Chem.* **2007,** *263* (1–2), 103-111.

16. (a) Malizia, F.; Fait, A.; Cruciani, G., *Chemistry – A European Journal* **2011,** *17* (49), 13892-13897; (b) Huang, R.; Malizia, F.; Pennini, G.; Koning, C. E.; Chadwick, J. C., *Macromol. Rapid Commun.* **2008,** *29* (21), 1732-1738; (c) Bart, J. C. J.; Roovers, W., *JOURNAL OF MATERIALS SCIENCE* **1995,** *30* (11), 2809-2820; (d) Forte, M. C.; Coutinho, F. M. B., *Eur. Polym. J.* **1996,** *32* (2), 223-231; (e) Buchacher, P.; Fischer, W.; Aichholzer, K. D.; Stelzer, F., *J. Mol. Catal. A: Chem.* **1997,** *115* (1), 163-171; (f) Stukalov, D. V.; Zakharov, V. A.; Potapov, A. G.; Bukatov, G. D., *J. Catal.* **2009,** *266* (1), 39-49.

17. Busico, V.; Corradini, P.; De Martino, L.; Proto, A.; Savino, V.; Albizzati, E., *Die Makromolekulare Chemie* **1985,** *186* (6), 1279-1288.

18. (a) Busico, V.; Cipullo, R.; Monaco, G.; Talarico, G.; Vacatello, M.; Chadwick, J. C.; Segre, A. L.; Sudmeijer, O., *Macromolecules* **1999,** *32* (13), 4173-4182; (b) Corradini, P.; Barone, V.; Guerra, G., *Macromolecules* **1982,** *15* (5), 1242-1245; (c) Liu, B.; Nitta, T.; Nakatani, H.; Terano, M., *Macromol. Chem. Phys.* **2003,** *204* (3), 395-402.

19. Mori, H.; Sawada, M.; Higuchi, T.; Hasebe, K.; Otsuka, N.; Terano, M., *Macromol. Rapid Commun.* **1999,** *20* (5), 245-250.

20. Oleshko, V. P.; Crozier, P. A.; Cantrell, R. D.; Westwood, A. D., *J. Electron Microsc.* **2002,** *51* (suppl 1), S27-S39.

21. Cheruvathur, A. V.; Langner, E. H. G.; Niemantsverdriet, J. W.; Thüne, P. C., *Langmuir* **2012,** *28* (5), 2643-2651.

22. Sozzani, P.; Bracco, S.; Comotti, A.; Simonutti, R.; Camurati, I., *J. Am. Chem. Soc.* **2003,** *125* (42), 12881-12893.

23. Magni, E.; Somorjai, G. A., *Surf. Sci.* **1997,** *377–379*, 824-827.

24. Brambilla, L.; Zerbi, G.; Piemontesi, F.; Nascetti, S.; Morini, G., *J. Phys. Chem. C* **2010,** *114* (26), 11475-11484.

25. (a) Corradini, P.; Guerra, G.; Fusco, R.; Barone, V., *Eur. Polym. J.*

1980, *16* (9), 835-842; (b) Corradini, P.; Busico, V.; Cavallo, L.; Guerra, G.; Vacatello, M.; Venditto, V., *J. Mol. Catal.* **1992,** *74* (1–3), 433-442.
26. Corradini, P.; Guerra, G.; Cavallo, L., *Acc. Chem. Res.* **2004,** *37* (4), 231-241.
27. D'Amore, M.; Credendino, R.; Budzelaar, P. H. M.; Causá, M.; Busico, V., *J. Catal.* **2012,** *286* (0), 103-110.
28. (a) Ehm, C.; Antinucci, G.; Budzelaar, P. H. M.; Busico, V., *J. Organomet. Chem.* **2014,** *772–773* (0), 161-171; (b) Correa, A.; Bahri-Laleh, N.; Cavallo, L., *Macromol. Chem. Phys.* **2013,** *214* (17), 1980-1989.
29. (a) Zhao, Y.; Schultz, N. E.; Truhlar, D. G., *Journal of Chemical Theory and Computation* **2006,** *2* (2), 364-382; (b) Zhao, Y.; Truhlar, D. G., *J. Chem. Phys.* **2006,** *125* (19), 194101; (c) Zhao, Y.; Schultz, N. E.; Truhlar, D. G., *J. Chem. Phys.* **2005,** *123* (16), 161103/1-161103/4; (d) Zhao, Y.; Truhlar, D., *Theor. Chem. Acc.* **2008,** *120* (1-3), 215-241.
30. (a) Grimme, S., *J. Comput. Chem.* **2004,** *25* (12), 1463-1473; (b) Grimme, S., *J. Comput. Chem.* **2006,** *27* (15), 1787-1799; (c) Grimme, S.; Antony, J.; Ehrlich, S.; Krieg, H., *J. Chem. Phys.* **2010,** *132* (15), -; (d) Grimme, S.; Ehrlich, S.; Goerigk, L., *J. Comput. Chem.* **2011,** *32* (7), 1456-1465.
31. (a) Busico, V.; Causà, M.; Cipullo, R.; Credendino, R.; Cutillo, F.; Friederichs, N.; Lamanna, R.; Segre, A.; Van Axel Castelli, V., *J. Phys. Chem. C* **2008,** *112* (4), 1081-1089; (b) Credendino, R.; Busico, V.; Causa, M.; Barone, V.; Budzelaar, P. H. M.; Zicovich-Wilson, C., *PCCP* **2009,** *11* (30), 6525-6532.
32. Donnay, J., D., H.; Harker, D., *Am. Mineral.* **1937,** *22*, 446.
33. Capone, F.; Rongo, L.; D'Amore, M.; Budzelaar, P. H. M.; Busico, V., *J. Phys. Chem. C* **2013,** *117* (46), 24345-24353.
34. Credendino, R.; Liguori, D.; Fan, Z.; Morini, G.; Cavallo, L., *ACS Catalysis* **2015,** *5* (9), 5431-5435.
35. Stukalov, D. V.; Zilberberg, I. L.; Zakharov, V. A., *Macromolecules* **2009,** *42* (21), 8165-8171.
36. Seth, M.; Margl, P. M.; Ziegler, T., *Macromolecules* **2002,** *35* (20), 7815-7829.
37. (a) Andoni, A.; Chadwick, J. C.; Niemantsverdriet, H. J. W.; Thüne, P. C., *J. Catal.* **2008,** *257* (1), 81-86; (b) Puhakka, E.; Pakkanen, T. T.; Pakkanen, T. A., *J. Mol. Catal. A: Chem.* **1997,** *123* (2–3), 171-178; (c) Cavallo, L.; Guerra, G.; Corradini, P., *J. Am. Chem. Soc.* **1998,** *120* (10), 2428-2436; (d)

Seth, M.; Ziegler, T. In *DFT-QM/MM examination of possible active sites in TiCl4/MgCl2 based heterogeneous Ziegler-Natta catalysts*, American Chemical Society: 2001; pp INOR-433.

38. (a) Auriemma, F.; Rosa, C. D., *Chem. Mater.* **2007,** *19* (24), 5803-5805; (b) Auriemma, F.; De Rosa, C., *J. Appl. Crystallogr.* **2008,** *41* (1), 68-82.

Chapter 2. A Cluster DFT-D Modelling Approach to ZNC

2.1 A difficult question: how small are primary $MgCl_2$ particles?

2.1.1 'Physical' vs 'Chemical' activation

As was recalled in the previous **Chapter**, present-day Ziegler-Natta $MgCl_2$/LB/$TiCl_4$ pre-catalysts consist of secondary aggregates of primary particles, with high surface area (typically > 50 m^2/g) and a controlled spherical morphology. The preferred technique to prepare such solids is precipitation from soluble precursor solutions (e.g. MgR_2 or $MgCl_2$/alcohol adducts), by reaction with a chlorinating agent which in most cases is $TiCl_4$.[1] According to the literature, these 'chemically activated' products are nano-structured, with average dimensions of the primary particles in the range of few nm, but often feature complex compositions, due to the residual presence of unreacted moieties and/or the formation of byproducts. This complicates attempts at experimental characterization and computational modelling.

The preparation of Ziegler-Natta pre-catalysts via physical activation can yield cleaner samples, provided that the reagents are pure enough and properly manipulated. Nowadays, highly efficient planetary ball-mills are capable of generating nano-structured materials in few hours, due to a mechanical energy 1000-fold larger than conventional ball-mills;[2] as a matter of fact, samples featuring primary particles of similar size compared with chemically activated ones can be obtained. The drawback of this route is the total loss of control over particle morphology; this

hampers any hypothesis of practical application, but is unimportant when modelling chemisorption phenomena, driven only by localized interactions.

2.1.2 Dehydration of $MgCl_2$

$MgCl_2$ is an extremely hygroscopic salt, and its lateral crystal terminations are normally saturated with chemisorbed H_2O, even when handled inside glove-boxes at very low water pressure (~10^{-5} bar). Measuring the H_2O content of such samples is exceedingly difficult, because further H_2O can be introduced throughout the analysis; in our experience, preparing suspensions in a heptane solution of Me_3Al and determining the amount of methane evolved via GC represents the safest approach (see **Appendix I** for details). Typically, H_2O contents between 0.1 ÷ 0.5 wt-% are found, which is consistent with the presence of chemisorbed water decorating the vast majority of the unsaturated $MgCl_2$ crystal edges.[3]

Commercial samples of 'dry' $MgCl_2$ often contain even greater H_2O amounts; as a matter of fact, the powder X-ray diffraction (XRD) patterns reveal the presence of several hydrated $MgCl_2 \bullet nH_2O$ crystal phases[4] (see **Figure 2.1-top**).

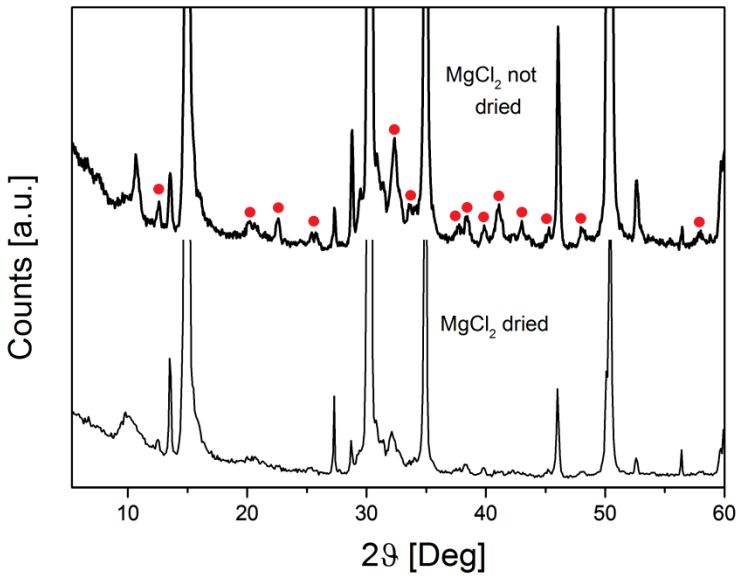

Figure 2.1 Powder XRD spectra of a commercial sample of 'dry' $MgCl_2$ before (top) and after (bottom) treatment with $SiCl_4$. The red dots indicate diffraction peaks due to various hydrated phases (see text).

In this work, we implemented a drying protocol based on the reaction with $SiCl_4$ in heptane solution (typically 1:2 v/v; see **Appendix II** for details); this leads to the formation of $HCl_{(g)}$ and a separate phase of SiO_2. XRD characterization of the recovered solid confirmed that the treatment is effective (**Figure 2.1-bottom**).

2.1.3 Measuring $MgCl_2$ nano-particle sizes from XRD patterns

$MgCl_2$ has a layered crystal structure characterized by polymorphism.[1a, 5] In all modifications, the common leitmotiv is a 'structural layer' made of two planes of close-packed Cl atoms with Mg atoms occupying all octahedral cavities in between. The lattice is obtained by the perpendicular stacking of the structural layers; in the stable α

modification, the succession of the Cl planes is $(ABC)_n$. The hexagonal unit cell features $\underline{a}$ = 0.364 nm, and $\underline{c}$ = 1.767 nm.[5]

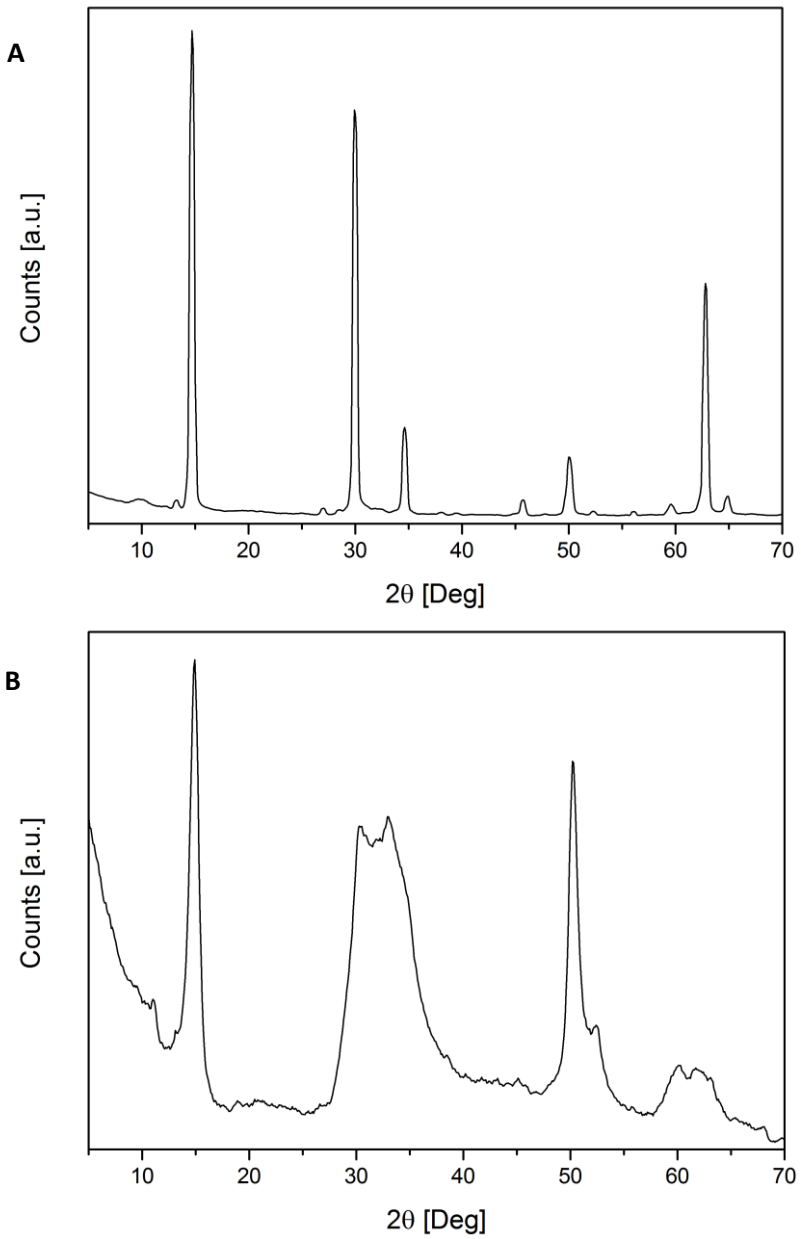

Figure 2.2 XRD patterns of dehydrated α-$MgCl_2$ before (**A**) and after (**B**) physical activation.

Planetary ball-milling of a dehydrated $MgCl_2$ sample for 8 hours changes the XRD profile as shown in **Figure 2.2**. In the ball-milled material, all diffraction peaks are considerably broadened, which can be traced to a strong decrease of average crystallite sizes and the introduction of structural disorder (typical of the so-called δ-$MgCl_2$ modification).[6]

According to Giunchi and Allegra,[6] the average dimensions of the crystallites along the $\underline{\boldsymbol{c}}$ and $\underline{\boldsymbol{a}}$ axes ($\langle L_c \rangle$ and $\langle L_a \rangle$, respectively) can be estimated from the full widths at half height of the 003 (2θ ~15.0°) and 110 (2θ ~50.1°) diffractions[1b] (I_1 and I_2, respectively), according to **Eqs. 2.1** and **2.2**:

$$\langle L_c \rangle = {}^{2\underline{\boldsymbol{c}}}\!/_{3\gamma} \qquad \textbf{Eq. 2.1}$$

$$\langle L_a \rangle = {}^{\underline{\boldsymbol{a}}}\!/_{\alpha} \qquad \textbf{Eq. 2.2}$$

In said equations, which are customized versions of the well-known Scherrer formula,[7] α and γ are empirical parameters obtained by linear regression on experimental data (**Figure 2.3**). Consequently, we reversed the work of the authors, obtaining α and γ using our experimental values and then we calculated the average dimensions of a $MgCl_2$ nano-particles with the two equations provided.

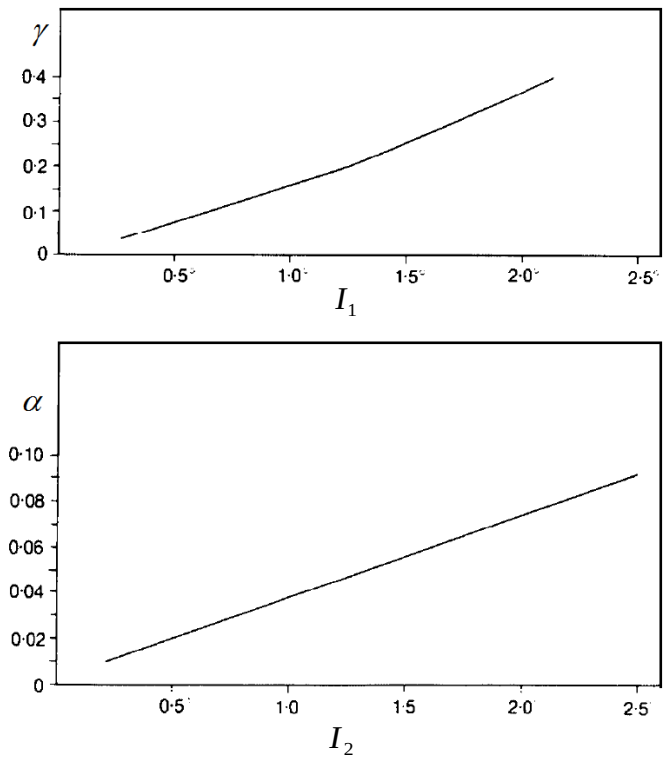

Figure 2.3 Correlation diagrams between I_1 and I_2 (in 2θ units) and the empirical parameters γ and α of **Eqs 2.1** and **2.2**.[6]

By applying this method to the spectrum of **Figure 2.2-B**, we concluded that in the specific ball-milled sample the primary particles had average dimensions around 13 nm both parallel and perpendicular to the structural layers. This result, which agrees with the previous literature,[3] is somewhat surprising in view of the known anisotropy of large(r) crystals, in which the weak Van der Waals assembly of the structural layers leads to a platelet morphology. On the other hand, computational studies of $MgCl_2$ surfaces concluded that lateral (104) and (110) terminations have a

relatively modest surface energy (~0.2 and ~0.4 J/m^2, respectively),[3] and the intensive planetary ball-milling process may well lead to metastable samples. Of course, these will tend to chemisorb Lewis Bases (H_2O in the first place) on the coordinatively unsaturated side edges to stabilize them. As a matter of fact, we observed that the physical activation of binary $MgCl_2$/ID systems (ID = diisobutyl phthalate, DIBP; 2,2-dimethyl-1,3-dimethoxypropane, DMMP) yields much smaller primary particles than neat $MgCl_2$, the more so the greater the ID/Mg mole ratio (**Table 2.1**). Average sizes of 4 ÷ 8 nm were typically achieved, with some samples approaching the mono-layer state; the latter finding, in particular, suggests that ID chemisorption favors exfoliation, likely due to steric repulsions pushing the layers apart and so lowering the inter-layer interactions. This interpretation is supported by the shift of the (003) diffraction to smaller 2θ angles, indicating a larger distance between adjacent structural layers (**Figure 2.4**).

Importantly, the same qualitative observations hold for industrial chemically activated ZN pre-catalysts.

Table 2.1 Average dimensions of the primary particles in planetary ball-milled neat $MgCl_2$ and $MgCl_2$/ID samples (in round brackets is the ID loading prior to final sample hot-washing).

Sample	Composition	*n* (ID)/*n* (Mg) [%]	$\langle L_a \rangle$	$\langle L_c \rangle$
1	$MgCl_2$	0.0	13.0	12.6
2	$MgCl_2$ / DIBP	2.1 (4.3)	7.8	7.3
3	$MgCl_2$ / DMMP	4.3 (4.3)	7.7	4.2
4	$MgCl_2$ / DIBP	6.7 (10.0)	3.9	n.d.
5	$MgCl_2$ / DMMP	10.0 (10.0)	4.4	2.8

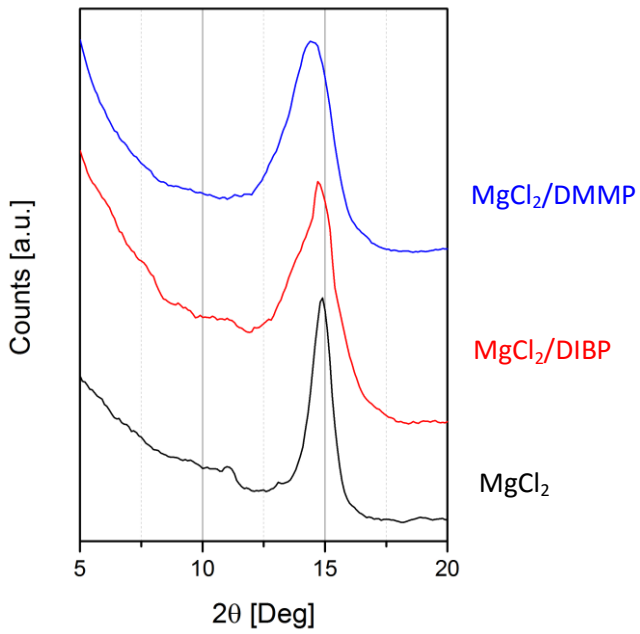

Figure 2.4 XRD spectra of samples **1**, **2** and **3** of **Table 2.1**, expanded in the region of the (003) diffraction.

2.2 Implementing a Cluster DFT-D Modelling Approach to ZNC

In view of the results of **§ 2.1** (and, more in general, of the previous literature), we believe that the computational modelling of ZNC active sites using periodic DFT-D codes is not the most appropriate strategy, and a cluster approach represents a more realistic approximation. According to the latter approach, $MgCl_2$ primary particles are modelled by means of finite single structural layers of appropriate sizes and morphology; the optimization of their structures, and the chemisorption of LB and $TiCl_4$ molecules on their lateral terminations, represent the subjects of the present **Chapter** and the following two, respectively. The main novelty of

our approach is that we considered fully relaxed structures, thus allowing for the local distortions expected for real systems. Great care was given to the level of theory to be used in order to achieve significant results; in particular, state-of-the-art DFT-D functionals were adopted (see next section for details).

The great flexibility of the approach (the number of structures that can be designed is huge) generates a problem of priority (what to model first). Moreover, each cluster structure is, in a way, unique, which complicates comparisons and identification of general trends. On the other hand, we verified that the local interactions involved in the chemisorption of individual molecules are almost unaffected by the specific structure of the cluster, as long as the nature of the Mg center(s) is the same (e.g. 5-coordinated or 4-coordinated), and the chemisorption site is not too close to highly defective locations such as corners (see section 2.3.2).

2.2.1 Theoretical methods: geometry optimization

In terms of DFT-D modelling, even a small $MgCl_2$ cluster is a fairly large system. Aiming to develop practical calculation protocols, we searched for the least time-demanding strategy still compatible with accurate structure and energy evaluations. All of the investigated structures were optimized using the Turbomole package (version 6.4),[8] employing the TPSS functional (defined in Turbomole as a Slater-Dirac LDA functional + TPSS for the exchange part and a Perdew-Wang 1992 LDA functional + TPSS for the correlation part),[9] and multiple grid size m4.[10] The

electronic configuration of all atoms was described by means of a split valence basis set plus polarization functions (labelled as def2-SVP in Turbomole).[11] The RI approximation[12] (with the def2-SVP auxiliary basis set),[10b, 13] combined with MARI-J accelerator,[14] was used for this part of the work. Vibrational analyses (numerical frequencies) were performed to confirm the absence of imaginary frequencies. Thermal contributions (enthalpy and entropy at 25°C) to binding energies were also calculated at this level.

To validate the protocol, a cluster of 20 $MgCl_2$ units exposing (mainly) 5-coordinate Mg atoms, thus mimicking 104 crystal terminations (Clu_104_20, **Figure 2.5**), was optimized using different combinations of basis sets and functionals, with and without accelerator (i.e. RI and MARI-J). In this phase, the M06 functional[15] (often highlighted for its reliability and accuracy) was also employed for comparative purposes; this functional is not implemented in the Turbomole 6.4 package, and therefore the Gaussian 09 package[16] had to be used.

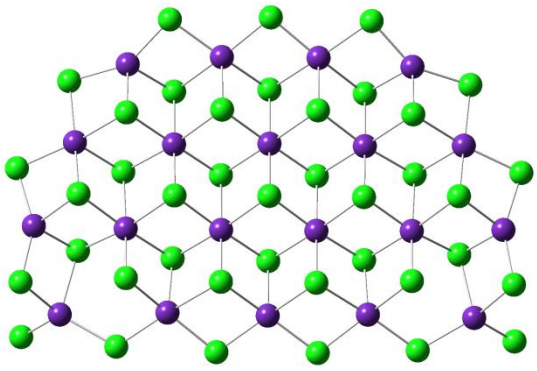

Figure 2.5 Optimized structure for CLU_104_20. Atom colors: Cl green, Mg violet.

Root Mean Square Displacement (RMSD) values for the optimized structures are very small (see **Table 2.2**), which indicates that they are all very similar. Therefore, we opted for the RI-TPSS/def2-SVP level of theory as the one associated with the lowest CPU-time. It is worth noting that the Turbomole package allows to execute this type of job on multiple nodes, a mandatory requirement to investigate a large number of systems in a reasonable time span.

Table 2.2 RMSD values measured for Clu_104_20 minima obtained using different optimization protocols.

Software	Level of theory	RMSD [Å]
Turbomole 6.4	RI-TPSS/def2-SVP	0.00
	TPSS/def2-SVP	0.27
	RI-TPSS/6-311G**	0.08
	B3LYP/TZVP	0.26
Gaussian 09	M06/SVP	0.14
	M06/TZVP	0.17
	M06/6-311G**	0.11

2.2.2 Theoretical methods: binding energy calculations

The optimized structures obtained at RI-TPSS/def2-SVP level of theory were used for binding energy evaluations by means of single point calculations, using the same functional but with a more expensive triple-ζ basis set (namely def2-TZVPP).[11] Also in this case, the aforementioned accelerators were applied (i.e. RI and MARI-J, as well as the multiple grid set). All binding energies were corrected for Basis Set Superposition Error (BSSE, according to the protocol of Boys and Bernardi)[17] and for dispersion (using Grimme's 2nd generation correction available in Turbomole, indicated from now on as D2).[18]

To evaluate the consistency of the results acquired, further single point calculations were carried out with the Gaussian 09 package in the framework of validation tests. In line with recently published protocols,[19] two functionals (i.e. TPSSTPSS[9d] with D2 corrections and M06-2X)[20] and two heavily polarized double-ζ basis sets (namely 6-31+G(2d,p)[21] and (m)aug-cc-pVDZ)[22] were adopted, thus generating a total of five binding energies for each structure optimized at a lower level of theory. All values turned out to be the same within the error bar of DFT methods (i.e. ±1.5 kcal/mol).[19c] For the sake of clarity, only results at RI-TPSS-D2/def2-TZVPP//RI-TPSS/def2-SVP level of theory will be reported in the following, unless indicated otherwise.

2.2.3 Design of $MgCl_2$ model clusters

To design our $MgCl_2$ model clusters, we started from a perfect single structural layer (monolayer), based on the crystal structure of the α phase.[23] Clusters with suitable sizes and shapes were cut out of said monolayer; as examples, Clu_104_24 and Clu_110_27 structures (**Figures 2.6**) consist of 24 and 27 $MgCl_2$ units and expose (mainly) 5-coordinated and 4-coordinated Mg atoms mimicking 104 and 110 crystal terminations, respectively. Despite the complete lack of constraints, both clusters remained compact upon structure optimization, although considerable reconstruction occurred at edges and/or corners (see also **Table 2.3**).

In the interior of Clu_104_24, bond lengths and angles turned out to be very close to those for an α-$MgCl_2$ crystal. On the other hand, the

5-coordinated Mg atoms on the surface underwent inwards displacements, developing a distorted square-pyramidal environment with average Cl-Mg-Cl angles around 160° (instead of 180° as in the perfect crystal). The corners were even more distorted, showing angles typical of a tetrahedral coordination geometry, and one Mg-Cl "bond" elongated up to 2.9 Å.

For Clu_110_27, in turn, inspection of the geometry shows that also the inner part of the cluster developed slight distortions compared with the perfect crystal. On the other hand, distortion along the edges was smaller than in Clu_104_24, indicating a more rigid environment of the 4-coordinated surface Mg atoms. Here too, the corners were heavily distorted, showing tetrahedral Mg bearing dangling chlorines.

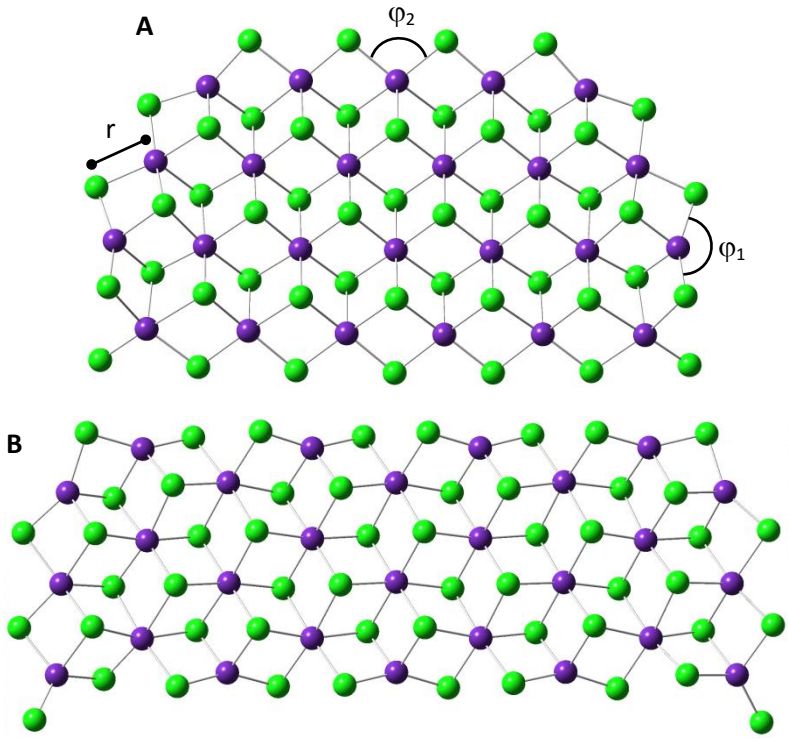

Figure 2.6 Optimized structures of Clu_104_24 (**A**) and Clu_110_27 (**B**).

Table 2.3 Structural comparison between a perfect $MgCl_2$ sheet and the two clusters shown in **Figure 2.6**. The symbol '÷' indicates an interval of values.

Structure		φ_1 [deg]	φ_2 [deg]	r [Å]
perfect $MgCl_2$ sheet		180	90	2.6
Clu_104_24	inside	170 ÷ 180	85 ÷ 90	2.5 ÷ 2.6
	edges	150 ÷ 165	90 ÷ 110	2.4 ÷ 2.6
Clu_110_27	inside	170 ÷ 178	80 ÷ 90	2.5 ÷ 2.6
	edges	155 ÷ 165	90 ÷ 95	2.3 ÷ 2.5

2.3 Testing the approach: adsorption of small probe molecules

Using the cluster models described in the previous section, we investigated the adsorption behavior of individual small LB molecules such as H_2O, NH_3 (as a prototype of N-donors),[24] EtOH and dimethylether, and compared them with the results of previous periodic DFT-D calculations.

2.3.1 Local distortions and surface stabilization

Not unexpectedly, the results of section 2.2.3 indicate that corners are the most defective cluster locations, and feature the most extensive distortions around Mg. Differences at such sites may correspond to alternative local minima with rather similar energy and low separation barriers. We found that "slipping" from one such minimum into another upon structure optimization can be induced by adsorption/desorption events, even at comparatively large distance; depending on the particular system being studied, the reconstruction may be reversible or "one-way". Therefore, much care is required when comparing calculated adsorption energies to ensure that this type of artefact does not contaminate the results.

As a case study, here we illustrate the adsorption and desorption of dimethylether (DME) onto the Clu_104_24 model. The values of DME adsorption (ΔH_{ads}) and desorption (ΔH_{des}) enthalpy (entries **1** and **2** of **Table 2.4**) were calculated according to **Eqs. 2.3** and **2.4** respectively:

$$\Delta H_{ads} = H_{add} - \left(H^0_{Clu} + H^0_{DME}\right) \qquad \textbf{Eq. 2.3}$$

$$\Delta H_{des} = \left(H^*_{Clu} + H^0_{DME}\right) - H_{add} \qquad \textbf{Eq. 2.4}$$

where H_{add} is the enthalpy of the optimized Clu_104_24/DME adduct (**Figure 2.7-A**); H^0_{Clu} and H^0_{DME} are the enthalpies of the neat cluster and free DME in their minimum geometries; H^*_{Clu} is the enthalpy of the (re)optimized cluster structure after DME desorption. In the absence of any reconstruction, ΔH_{ads} = - ΔH_{des} (since $H^0_{Clu} = H^*_{Clu}$). Instead, the two values turned out to differ by 6.2 kcal/mol, indicating that DME binding made the cluster move from one local minimum to another (RMSD is 0.45 Å). Different entropy contributions were also involved in the process.

Table 2.4 Adsorption and desorption energies of DME on a neat (entries **1** and **2**) and H_2O-stabilized (entries **1**^{I} and **2**^{I}) Clu_104_24 model cluster (see text).

Entry	$\Delta H_{ads} \div \Delta H_{des}$ [kcal/mol]	$\Delta G_{ads} \div \Delta G_{des}$ [kcal/mol]
1	-25.6	-13.1
2	+19.4	+9.0
1^{I}	-19.4	-8.7
2^{I}	+19.7	+9.8

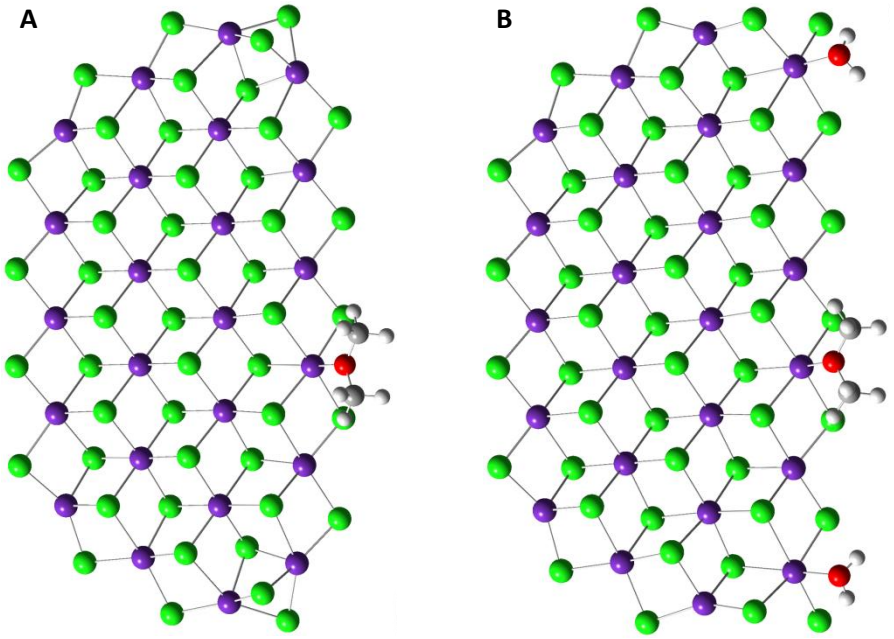

Figure 2.7 Optimized structures of the Clu_104_24/DME adduct without (**A**) and with (**B**) corner stabilization by chemisorbed H_2O (see text).

Due to the high affinity of $MgCl_2$ for H_2O and alcohols,[25] it seems reasonable to assume that the most unstable environments in a real primary particle would be covered by these molecules (or other LBs), even if they are present in the system at very low concentration. In order to 'freeze' rearrangements at corners, we explored the effects of stabilization by chemisorbed H_2O (**Figure 2.7-B**); our educated guess was that more 'saturated' systems should suffer less from the multiple minima problem. Therefore, we calculated ΔH and ΔG for DME adsorption/desorption on Clu_104_24 with H_2O-stabilized corners (entries **1'** and **2'** of **Table 2.4**). In line with our hypothesis, the results make it clear that the stabilized cluster did not undergo any appreciable reconstruction phenomenon.

One could argue that therefore the "best" models would have virtually all unsaturated sites covered by some kind of donor molecule. Unfortunately, this introduces so many additional degrees of freedom that the approach becomes unmanageable. In addition, most donor molecules come with their own alternative conformations (such as H bonding to neighboring Cl atoms or dipole interactions), replacing one source of artefacts by another. Therefore, we only used H_2O chemisorption at corners where this was necessary to prevent reconstruction in comparative adsorption studies.

2.3.2 Effects of cluster size on binding energy

To evaluate any dependence of adsorption energy on cluster size, we calculated ΔH_{ads} and ΔG_{ads} for the chemisorption of H_2O on model clusters with edges of different length (i.e. different number of $MgCl_2$ units). Based on the results in **Charts 2.1-A** and **2.1-B**, the effect is modest; indeed, ΔG_{ads} estimated using clusters of 10 to 40 $MgCl_2$ units turned out to be -9 kcal/mol and -12 kcal/mol at 5-coordinated and 4-coordinated Mg sites, respectively.

Chart 2.1 Values of enthalpy (black) and Gibbs free energy (red) for the adsorption of H_2O on Clu_104 (**A**) and Clu_110 (**B**) type clusters. All models exposing 5-coordinated Mg sites were stabilized.

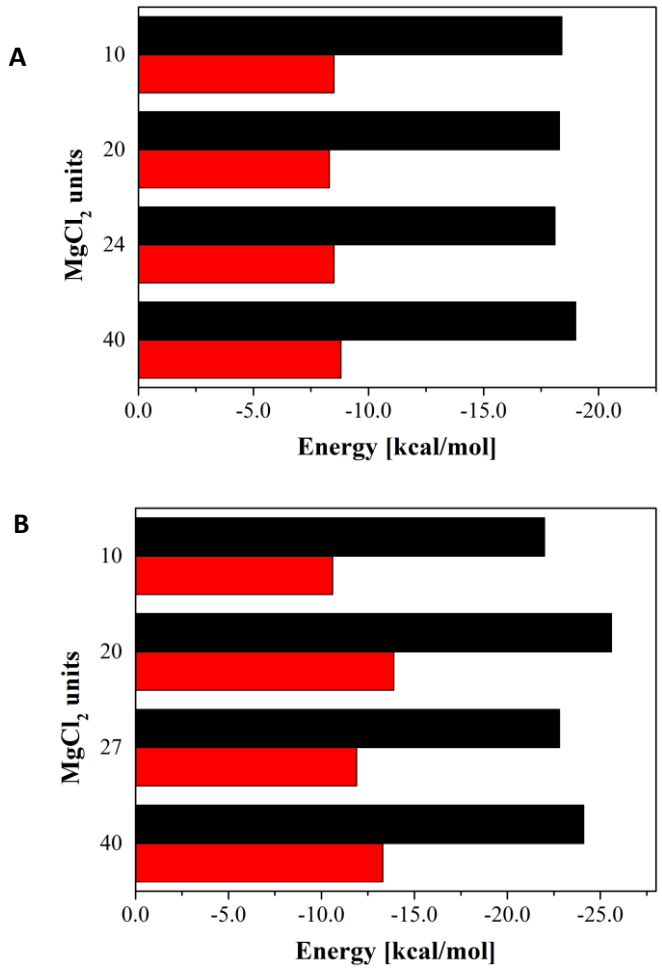

It is worth noting that the smallest cluster exposing 5-coordinated Mg was so tiny that even the binding of one single H_2O molecule was able to strongly distort it. We stabilized this cluster in two different ways, i.e. by binding two extra H_2O molecules (a) at the corners of the edge hosting the chemisorption site, or (b) at first-neighboring Mg atoms towards the

opposite edge (**Figure 2.8**). In the former case, the optimized geometry revealed the effect of weak repulsive dipole interactions between adjacent H_2O molecules (δ^+/δ^+ repulsion); this was not an issue in the latter case because the H_2O molecules are much further apart. Nevertheless, the calculated values of ΔH_{ads} and ΔG_{ads} were similar (within ~1 kcal/mol), and still close to those for larger clusters.

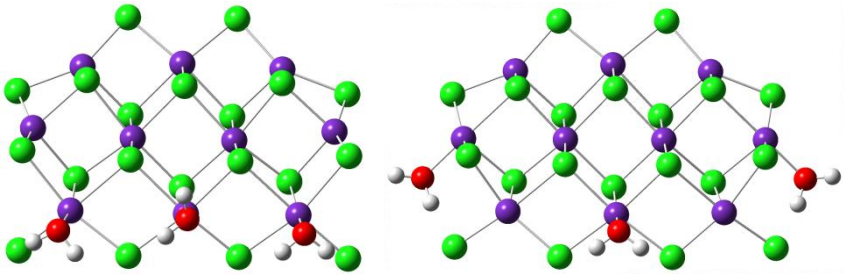

Figure 2.8 Different modes of stabilization by extra-chemisorbed H_2O of a Clu_104_10/H_2O adduct (see text).

2.3.3 Comparison between Cluster and Periodic DFT-D approaches

In the last part of this **Chapter**, we compare the results of the newly implemented Cluster approach with those of previously published Periodic DFT-D calculations for the adsorption of three small probe LBs, namely NH_3, EtOH, and H_2O.[26] Generally speaking, the two approaches provide similar chemical scenarios for homologous systems (**Table 2.5**). Both assign a higher Lewis acidic character to 4-coordinated surface Mg atoms relative to 5-coordinated ones. However, modest but not insignificant differences in ΔH_{ads} and ΔG_{ads} energies are seen.

Table 2.5 Enthalpy and Gibbs free energies of adsorption of small LB probes on Clu_104 and Clu_110 models (more specifically Clu_104_24 and Clu_110_27) compared with corresponding values obtained by periodic DFT-D calculations.[26]

Entry	Structure	ΔH_{ads} [kcal/mol]	ΔG_{ads} [kcal/mol]
1	Clu_104 / NH_3	-25.3	-15.1
2	Clu_110 / NH_3	-28.3	-17.3
1^{I}	Per_104 / NH_3	-19.5	-9.4
2^{I}	Per_110 / NH_3	-30.2	-19.4
3	Clu_104 / EtOH	-21.4	-11.1
4	Clu_110 / EtOH	-26.0	-15.3
3^{I}	Per_104 / EtOH	-16.8	-5.7
4^{I}	Per_110 / EtOH	-25.8	-14.5
5	Clu_104 / H_2O	-18.6	-9.0
6	Clu_110 / H_2O	-22.8	-11.9
5^{I}	Per_104 / H_2O	-18.6	-8.7
6^{I}	Per_110 / H_2O	-28.3	-17.7

Indeed, by definition our cluster approach ignores all interactions (both stabilizing and destabilizing) between the adsorbate and Cl atoms belonging to contiguous layers of $MgCl_2$, so that binding energies may come out either too low or too high. Our results suggest that – at least for small adsorbate molecules – missing the stabilizing interactions is the larger error, and hence cluster calculations underestimate binding somewhat (see e.g. **Figure 2.9-C** and entries **6** and **6**^{I} of **Table 2.5**); whether this is desirable or not depends on the nature of the particle modelled (monolayer or stack). Due to the inherent nature of the periodic description, on the other hand, the results overestimate the contribution of long-range interactions; in fact, the strict 2D periodical order on a fully (or densely) covered surface forces each molecule of adsorbate to interact

with copies of itself. For instance, short H-H distances between adjacent molecules (i.e. 2.2 ÷ 2.7 Å) were observed in the periodic model for the adsorption of EtOH on $MgCl_2$(104) (entry **3**^{I} of **Table 2.5** and **Figure 2.9-A**). Moreover, the orientations of NH_3 and H_2O molecules on the same surface suggest dipole-dipole interactions resulting into rather different structures compared to mono-adsorption models within the cluster approach (**Figure 2.9-B**).

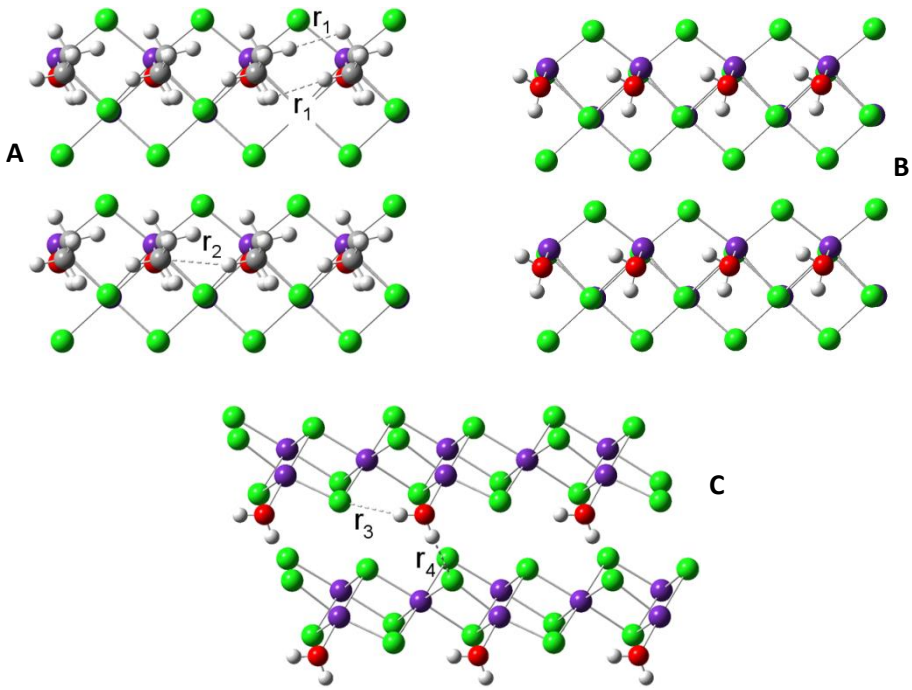

Figure 2.8 Periodic DFT-D models for adsorption of EtOH (**A**) and H_2O (**B** and **C**) on α-$MgCl_2$(104) and α-$MgCl_2$(110) surfaces.[45] r_1 = 2.20 Å, r_2 = 2.67 Å, r_3 = 2.33 Å, r_4 = 2.70 Å. The Van der Waals radii for H, C and Cl are respectively 1.20 Å, 1.70 Å and 1.75 Å.

Deciding which model is "best" is not trivial, and depends on the specific case of interest. The periodic approach is closer to a fully donor-covered surface, while the cluster model gives the cleanest picture of how a single donor molecule interacts with a given surface. It is plausible that the adsorption energy of a LB molecule on a real primary particle of $MgCl_2$ lies somewhere in between the values calculated in the framework of the two approaches.

References

1. (a) Moore, E. P., Jr., Ed., *Polypropylene Handbook: Polymerization, Characterization, Properties, Processing, Applications*. Hanser Publishers: Munich, Germany: 1996; (b) Auriemma, F.; De Rosa, C., *J. Appl. Crystallogr.* **2008,** *41* (1), 68-82; (c) Huang, R.; Malizia, F.; Pennini, G.; Koning, C. E.; Chadwick, J. C., *Macromol. Rapid Commun.* **2008,** *29* (21), 1732-1738; (d) Malizia, F.; Fait, A.; Cruciani, G., *Chemistry – A European Journal* **2011,** *17* (49), 13892-13897.

2. Chen, Y.; Li, C. P.; Chen, H.; Chen, Y., *Science and Technology of Advanced Materials* **2006,** *7* (8), 839-846.

3. Busico, V.; Causà, M.; Cipullo, R.; Credendino, R.; Cutillo, F.; Friederichs, N.; Lamanna, R.; Segre, A.; Van Axel Castelli, V., *J. Phys. Chem. C* **2008,** *112* (4), 1081-1089.

4. Sugimoto, K.; Dinnebier, R. E.; Hanson, J. C., *Acta Crystallographica Section B* **2007,** *63* (2), 235-242.

5. Partin, D. E.; O'Keeffe, M., *J. Solid State Chem.* **1991,** *95* (1), 176-183.

6. Giunchi, G.; Allegra, G., *J. Appl. Crystallogr.* **1984,** *17* (3), 172-178.

7. (a) Jenkins, R.; Snyder, R.; Editors, *Introduction to X-Ray Powder Diffractometry*. Wiley: 1996; p 544 pp., (approx.); (b) Cullity, B. D.; Stock, S. R., *Elements of X-Ray Diffraction (3rd Edition)*. Prentice Hall: 2001.

8. Ahlrichs, R.; Bär, M.; Häser, M.; Horn, H.; Kölmel, C., *Chem. Phys. Lett.* **1989,** *162* (3), 165-169.

9. (a) Dirac, P. A. M., *Quantum Mechanics of Many-Electron Systems*. 1929; Vol. 123, p 714-733; (b) Slater, J. C., *Physical Review* **1951,** *81* (3), 385-390; (c) Perdew, J. P.; Wang, Y., *Physical Review B* **1992,** *45* (23), 13244-13249; (d) Tao, J.; Perdew, J. P.; Staroverov, V. N.; Scuseria, G. E., *Phys. Rev. Lett.* **2003,** *91* (14), 146401.

10. (a) Treutler, O.; Ahlrichs, R., *J. Chem. Phys.* **1995,** *102* (1), 346-354; (b) Eichkorn, K.; Weigend, F.; Treutler, O.; Ahlrichs, R., *Theor. Chem. Acc.* **1997,** *97* (1-4), 119-124.

11. Weigend, F.; Ahlrichs, R., *PCCP* **2005,** *7* (18), 3297-3305.

12. (a) Von Arnim, M.; Ahlrichs, R., *J. Comput. Chem.* **1998,** *19* (15), 1746-1757; (b) Ahlrichs, R., *PCCP* **2004,** *6* (22), 5119-5121.

13. (a) Eichkorn, K.; Treutler, O.; Öhm, H.; Häser, M.; Ahlrichs, R., *Chem.*

Phys. Lett. **1995,** *242* (6), 652-660; (b) Weigend, F., *PCCP* **2006,** *8* (9), 1057-1065.

14. Sierka, M.; Hogekamp, A.; Ahlrichs, R., *J. Chem. Phys.* **2003,** *118* (20), 9136-9148.

15. (a) Zhao, Y.; Truhlar, D., *Theor. Chem. Acc.* **2008,** *120* (1-3), 215-241; (b) Zhao, Y.; Truhlar, D. G., *Chem. Phys. Lett.* **2011,** *502* (1–3), 1-13.

16. Hohenberg, P.; Kohn, W., *Physical Review* **1964,** *136* (3B), B864-B871.

17. Boys, S. F.; Bernardi, F., *Mol. Phys.* **1970,** *19* (4), 553-566.

18. Grimme, S., *J. Comput. Chem.* **2006,** *27* (15), 1787-1799.

19. (a) D'Amore, M.; Credendino, R.; Budzelaar, P. H. M.; Causá, M.; Busico, V., *J. Catal.* **2012,** *286* (0), 103-110; (b) Correa, A.; Bahri-Laleh, N.; Cavallo, L., *Macromol. Chem. Phys.* **2013,** *214* (17), 1980-1989; (c) Ehm, C.; Antinucci, G.; Budzelaar, P. H. M.; Busico, V., *J. Organomet. Chem.* **2014,** *772–773* (0), 161-171; (d) Ehm, C.; Budzelaar, P. H. M.; Busico, V., *J. Organomet. Chem.* **2015,** *775* (0), 39-49.

20. Zhao, Y.; Truhlar, D. G., *J. Chem. Phys.* **2006,** *125* (19), 194101.

21. Hehre, W. J.; Ditchfield, R.; Pople, J. A., *J. Chem. Phys.* **1972,** *56* (5), 2257-2261.

22. (a) Papajak, E.; Leverentz, H. R.; Zheng, J.; Truhlar, D. G., *Journal of Chemical Theory and Computation* **2009,** *5* (5), 1197-1202; (b) Papajak, E.; Truhlar, D. G., *Journal of Chemical Theory and Computation* **2010,** *6* (3), 597-601.

23. Dorrepaal, J., *J. Appl. Crystallogr.* **1984,** *17* (6), 483.

24. (a) Tritto, I.; Locatelli, P.; Sacchi, M. C. In *Study on the effects of the amines on the supported and traditional Ziegler-Natta catalysts*, Cambridge Univ. Press: 1988; pp 255-65; (b) Brita, D.; Casalini, A.; Evangelisti, D.; Fusco, O.; Collina, G. Magnesium dichloride-based adducts and catalyst components obtained therefrom. WO2004054711A1, 2004; (c) Shamshoun, E. S.; Lopez, M.; Chen, H. Supported modified Ziegler-Natta catalyst component, preparation thereof and polymerization using the same. EP1031581A1, 2000.

25. (a) Wu, X.; Xu, X., *Huaxue Xuebao* **2009,** *67* (6), 535-540; (b) Wu, X.; Song, L.; Pan, Y., *Huaxue Tongbao* **2010,** *73* (3), 246-251; (c) Callahan, K. M.; Casillas-Ituarte, N. N.; Roeselová, M.; Allen, H. C.; Tobias, D. J., *J. Phys. Chem. A* **2010,** *114* (15), 5141-5148.

26. Capone, F.; Rongo, L.; D'Amore, M.; Budzelaar, P. H. M.; Busico, V., *J. Phys. Chem. C* **2013,** *117* (46), 24345-24353.

Chapter 3. Adsorption of industrial Lewis Bases

3.1 Experimental facts

All industrial Ziegler-Natta pre-catalysts contain a Lewis Base (the so-called Internal Donor, ID) in significant amounts (10 ÷ 20 wt-%); as noted in **Chapter 1**, this is mandatory to achieve a high stereoselectivity in propene polymerization.[1] Effective IDs include aromatic monoesters (e.g. alkyl benzoates), aromatic diesters (e.g. dialkyl phthalates), aliphatic diesters (e.g. diethyl 2,3-dialkylsuccinates) and 1,3-diethers (e.g. 2,2-dialkyl-1,3-dimethoxy-propanes). A second LB (the so-called External Donor, ED, which almost invariably is an alkoxysilane) is usually added to the R_3Al co-catalyst, to further enhance the stereoselectivity.[1c, 2] Although the role of such molecules is still under debate, it is a fact that practically all aspects of catalyst performance depend on the choice of the ID/ED pair. Therefore, it seems plausible that LB molecules chemisorbed on the surface of $MgCl_2$ at non-bonded contact with the active Ti species modulate the catalytic pocket by means of steric and (possibly) electronic effects, similarly to ancillary ligands in molecular catalysts.[3]

It has long been proposed, initially based on Molecular Mechanics (MM) and later on DFT calculations, that some IDs have a more or less strong preference for certain $MgCl_2$ crystal terminations; in particular, 1,3-diethers are believed to bind much more strongly to 4-coordinated Mg atoms (e.g. on $MgCl_2$(110) surfaces),[3b, 4] in the so-called chelating mode

(**Figure 3.1-A**). Others, instead, like phthalates and succinates, seem to adsorb rather indiscriminately on 5-coordinated and 4-coordinated Mg,[5] because they can adopt either a chelating or a bridging adsorption mode (**Figure 3.1-B**, **C** and **D**).[3b]

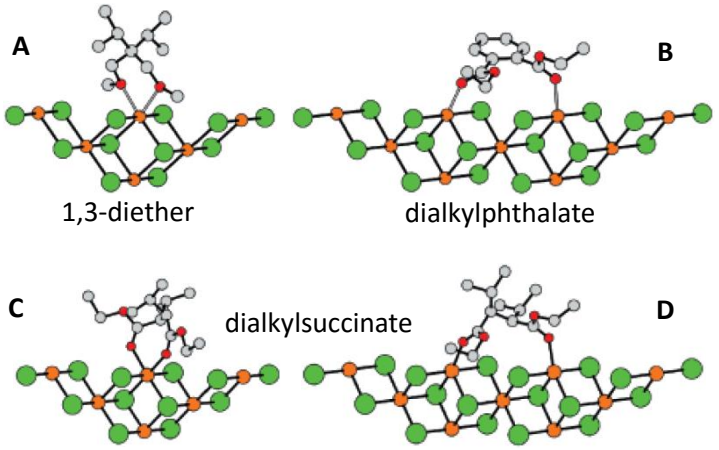

Figure 3.1 Schematic representations of binding modes of different IDs on a $MgCl_2$(110)-like surface.[3b]

Experimental evidence has been reported that ID and ED molecules are adsorbed on the support independently of $TiCl_4$. As we shall see in **Chapter 5**, computational data agree with such an interpretation. On the other hand, chemically activated Ziegler-Natta pre-catalysts are precipitated in the presence of the ID, which implies that in case the latter favors a certain $MgCl_2$ surface crystal morphology can be affected.

In the present work, we investigated the adsorption of some typical IDs (namely, 2,2-dimethyl-1,3-dimethoxypropane, DMMP; dibutyl phthalate, DBP; diisobutyl phthalate, DIBP) on pre-formed physically activated $MgCl_2$. To this end, the ID was added in variable amounts to a suspension of the ball-milled support in heptane (see **Appendix IV** for the

experimental protocol). The results, shown in **Figure 3.2**, highlighted drastically different behaviors; as a matter of fact, DMMP reached a saturation value already at fairly low ID/Mg mole ratio, whereas the adsorption of the two phthalates turned out to be much more extensive; in particular, DBP featured a linear dependence of ID uptake on ID/Mg mole ratio in solution up to very large values. Our interpretation of the above findings is that the diether ID adsorbed on the available coordinatively unsaturated (most likely, 4-coordinated) Mg atoms, whereas DBP behaved as a solvent, generating additional surface and, possibly, forming crystalline $MgCl_2$•DBP complexes. DIBP, in turn, featured an intermediate behavior; we trace the lower uptake compared with DBP to a greater steric demand. If said interpretation is correct, the implication is that caution is mandatory when investigating and modelling ID/$MgCl_2$ interactions.

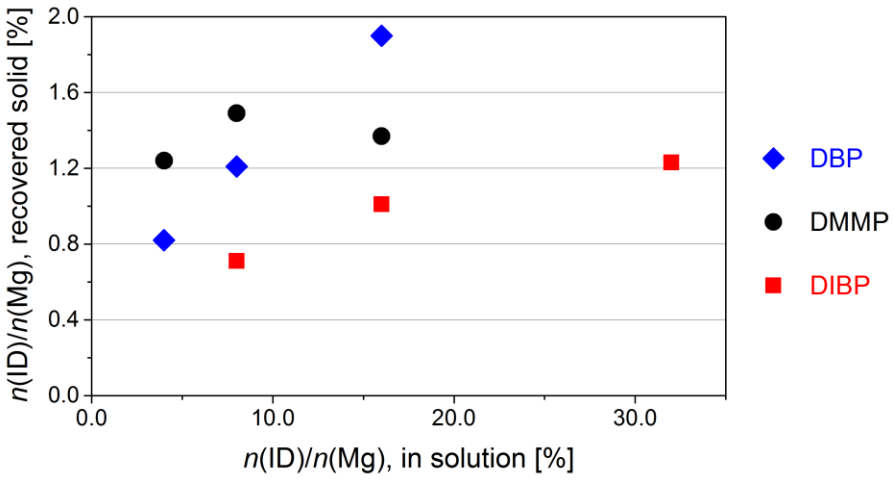

Figure 3.2 Correlation between ID/Mg mole ratio in solution and in the recovered solid for adsorption experiments of three different IDs on physically activated $MgCl_2$ in heptane suspension.

3.2 Computational study

3.2.1. Setting up the approach

The Cluster Approach described in **Chapter 2** was applied to study the chemisorption of representative ID and ED molecules on the lateral terminations of $MgCl_2$ model clusters. Compared with the few previous computational studies of similar kind,[3b, 6] the main elements of novelty of the present one were the lack of constraints on the examined structures, and the accurate evaluation of ΔG_{ads} (rather than ΔH_{ads} only). Our general aim was to attach a quantitative meaning to several long-standing qualitative hypotheses on donor binding, leading to the identification of the most plausible ones.

Clusters Clu_104_24 and Clu_110_27 (**Chapter 2**) were used as the substrates. As already explained, these structures expose 5-coordinate and 4-coordinate Mg atoms, locally representative of well-formed $MgCl_2$(104) and $MgCl_2$(110) surfaces, respectively. Both of them are large enough to feature adsorption sites which are comparatively far (~6 Å or more) from the heavily distorted cluster corners. The impact of the latter locations on structure optimization, and the possible need to stabilize them by means of H_2O adsorption, were discussed in section 2.3.1; for the purpose of the present **Chapter**, this was indeed necessary for Clu_104_24.

3.2.2 Aromatic monoester IDs

The first ID molecules to be considered in this investigation were methyl and ethyl benzoate (from here on, MeBz and EtBz, respectively). EtBz, in particular, was the ID employed in so-called 3rd-generation ZNC, the first $MgCl_2$-supported ones to be introduced in the iPP industry in the early 1970s.[1a, 7]

Based on IR and NMR data, it has been suggested that these molecules bind to the $MgCl_2$ surface with the carbonyl moiety in monodentate fashion, or with both O atoms of the ester group in bidentate fashion;[8] Zakharov,[6c] in particular, concluded that the latter binding mode is preferred, and leads to a fairly rigid adduct.

In **Figure 3.3** we show the two different conformers of MeBz and EtBz. In both cases, the planar conformation (**A**, **A**^{I}) is more stable, but can bind to the surface with the carbonyl O only; the non-planar one (**B**, **B**^{I}), in turn, is higher in energy by ~9 kcal/mol (due to the breakage of the extended π-system conjugation), but can bring both O atoms in contact with the surface.

Preliminary evaluations of adsorption energy in monodentate and bridging mode clearly indicated that the latter is not competitive, because the higher conformational energy is not compensated by any significant gain in the binding interaction. Therefore, we focused exclusively on the planar conformer.

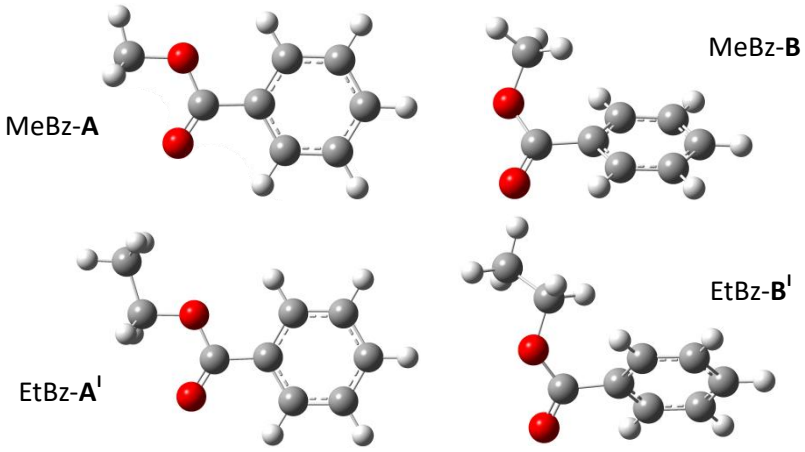

Figure 3.3 Planar (**A** and **A**^{I}) and non-planar (**B** and **B**^{I}) conformers of MeBz and EtBz.

Adduct formation led to a limited reconstruction, originating from the interplay of stabilizing interactions (primarily, short H-Cl contacts)[9] and destabilizing interactions (steric repulsions). This, however, did not cause any major changes in cluster structure; as a matter of fact, when the adsorbate was removed and the isolated clusters re-optimized, their structure returned to the original ones.

Several local minima differing in the relative orientation between cluster edge and adsorbate were identified for adsorption on Clu_104_24, depending on whether the torsion angle ϑ is ~ ±90° (**Figure 3.4-A**), ~0° or ~+180° (**Figure 3.4-B**).

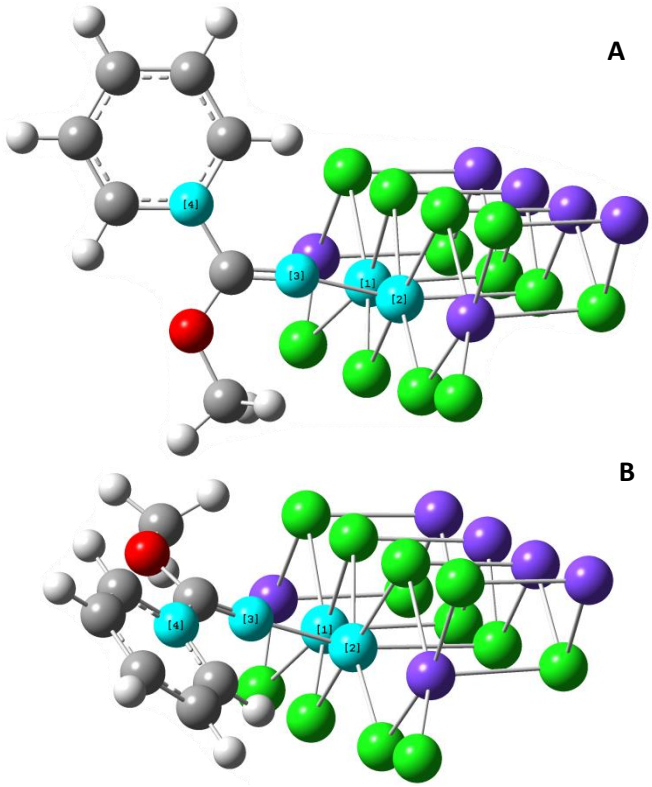

Figure 3.4 Different orientations of MeBz bound to a 5-coordinated Mg of Clu_104_24. The torsion angle ϑ is defined by atoms 1, 2 (= Mg), 3 (= O) and 4 (=C).

A notable difference between these two sets emerged in their vibrational behavior (which was studied in order to calculate the full entropy correction and therefore the adsorption free energy). In particular, the rocking vibration of the whole donor within its plane of symmetry around the Mg–O bond (**Figure 3.5**) in orientations with ϑ = ~0° or ~+180° is prevented by Cl atoms in close proximity to the adsorption site. This been said, the calculated values of adsorption energy for MeBz were all within ~1 kcal/mol (entries **1-4** of **Table 3.1**). The larger size of ethyl vs

methyl turned out to de-stabilize one of the 4 aforementioned orientations, to the point that the corresponding minimum could not be located (entries **1**^{I}-**3**^{I} of **Table 3.1**).

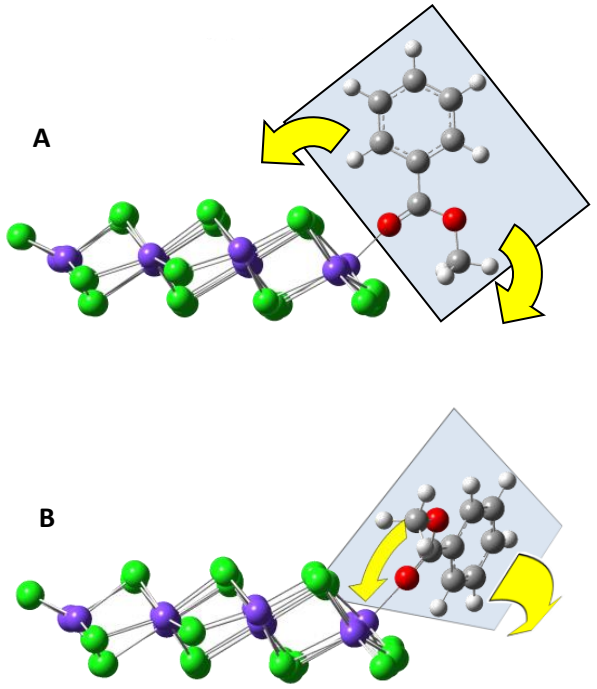

Figure 3.5 Rocking vibration mode around the Mg-O bond of the whole donor on its plane of symmetry. **A**: ϑ = +90°; **B**: ϑ = +180°.

Table 3.1 Binding energies of MeBz and EtBz on Clu_104_24. On the left, diagram of adsorbate displacement with respect to the ϑ torsion angle (see text).

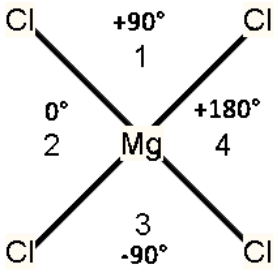

Entry	Structure	ΔH_{ads} [kcal/mol]	ΔG_{ads} [kcal/mol]
1	Clu_104_24 / MeBz	-23.5	-12.4
2	Clu_104_24 / MeBz	-22.7	-11.9
3	Clu_104_24 / MeBz	-23.8	-13.3
4	Clu_104_24 / MeBz	-23.8	-12.4
1^{I}	Clu_104_24 / EtBz	-23.5	-12.5
2^{I}	Clu_104_24 / EtBz	-23.6	-12.7
3^{I}	Clu_104_24 / EtBz	-24.7	-13.9

Concerning adsorption on Clu_110_27, we found that the donor can project either the methyl or the phenyl group towards the edge of the cluster (**Table 3.2**). The calculated values of adsorption energy turned out to be slightly stronger (>2 kcal/mol) than for Clu_104_24; this is consistent with the more open coordination site and the higher Lewis acidity of 4-coordinated Mg.

Table 3.2 Binding energies of MeBz and EtBz on Clu_110_27.

Entry	Structure	ΔH_{ads} [kcal/mol]	ΔG_{ads} [kcal/mol]
1	Clu_110_27 / MeBz	-26.4	-14.5
2	Clu_110_27 / MeBz	-26.0	-16.7
1^{I}	Clu_110_27 / EtBz	-27.0	-16.5
2^{I}	Clu_110_27 / EtBz	-26.9	-16.6

In both cases, monodentate ligation of an individual molecule resulted into a rather flexible binding, seemingly in contrast with the rigid environment claimed by literature IR and NMR studies. In real Ziegler-Natta pre-catalysts, on the other hand, the degree of surface coverage is high, and short distances between adjacent donor molecules may well justify a high local rigidity; in particular, at such high coverage structures featuring ϑ = 0° or +180° appear to be hampered.

3.2.3 Diester IDs

In the 1980s, EtBz-containing 3rd-generation ZNC were largely replaced by so-called 4th-generation ones, modified with dialkyl phthalate IDs;[10] these catalysts are much more active and stereoselective, although an ED is still required for optimal performance. More recently (early 2000s),[11] catalysts containing aliphatic diesters (e.g. dialkyl succinates) were also introduced, mainly because they yield polymers with a very broad molar mass distribution, of use for some applications.

For our investigation, we selected dimethyl phthalate (DMP) and dimethyl 2,3-dimethylsuccinate (DMSuc) as prototypical examples of the two aforementioned ID classes. Despite the common diester nature, the two molecules featured completely different behaviors.

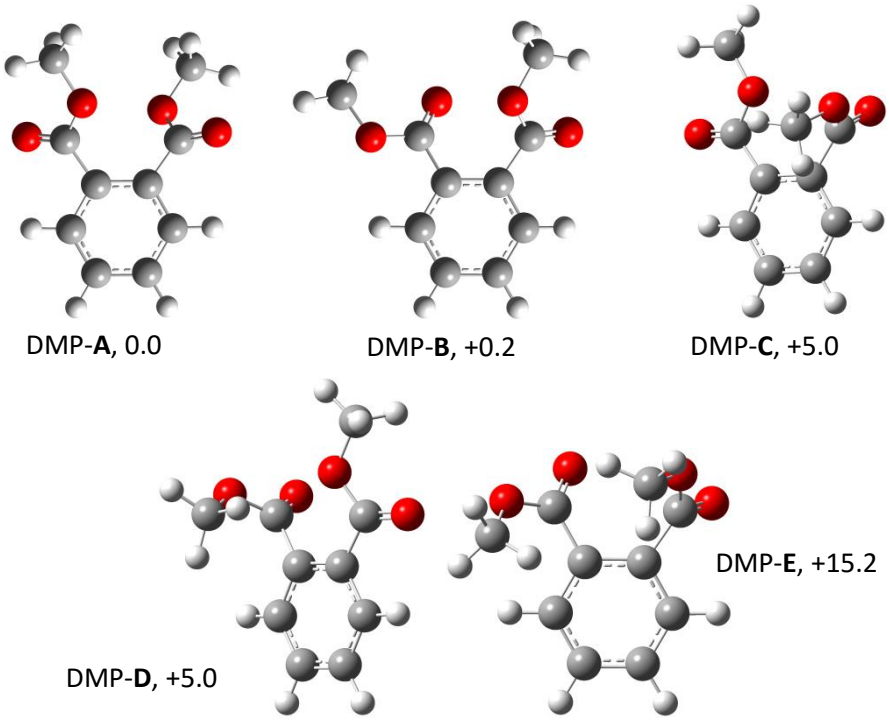

Figure 3.6 Different DMP conformers with relative electronic energy values (in kcal/mol).

In the case of DMP, out of five possible conformers, two (**A** and **B** in **Figure 3.6**) turned out to be lower in electronic energy by more than 5 kcal/mol than the remaining three (**C-E** in **Figure 3.6**); therefore, the latter were not considered further.

Conversely, DMSuc showed a much higher flexibility, with several conformers obtained by rotating skeletal single bonds featuring very similar values of electronic energy (**Table 3.3**; the various sets correspond to different chiralities of the stereogenic C's). In this case we considered only low energy conformations in which both carbonyl groups point to the same direction, and therefore can adopt the chelating and/or the bridging binding mode.

Table 3.3 Relative electronic energies of DMSuc conformers. **M** = meso form; **R** = 2(R),3(R) enantiomer; **S** = 2(S),3(S) enantiomer.

Structure	Relative electronic energy [kcal/mol]
DMSuc-**M1**	0.0
DMSuc-**M2**[a]	+0.7
DMSuc-**M2**[a]	+0.9
DMSuc-**M3**	+13.2
DMSuc-**R1**	0.0
DMSuc-**R2**[a]	+0.2
DMSuc-**R2**[a]	+0.4
DMSuc-**R2**[a]	+17.6
DMSuc-**R3**	+0.2
DMSuc-**S1**	0.0
DMSuc-**S2**	+0.8
DMSuc-**S3**[a]	+0.3
DMSuc-**S3**[a]	+1.1

[a] Structures with different orientation of carbonyl groups.

3.2.3.1 DMP adsorption modes

Out of the two low-energy conformers (**Figure 3.6**), only DMP-**B** can chelate a 4-coordinated Mg atom (e.g. of Clu_110_27) using both carbonyl O atoms; DMP-**A**, instead, should use one carbonyl O and the ether O of the other ester group, which results into a weaker binding (**Figure 3.7**). The so-called bridging mode on the same $MgCl_2$(110)-like edge, in turn, was only obtained with DMP-**B**; as a matter of fact, in the adducts with DMP-**A** only one carbonyl O turned out to bind, ending up with a situation similar to that for monoesters.

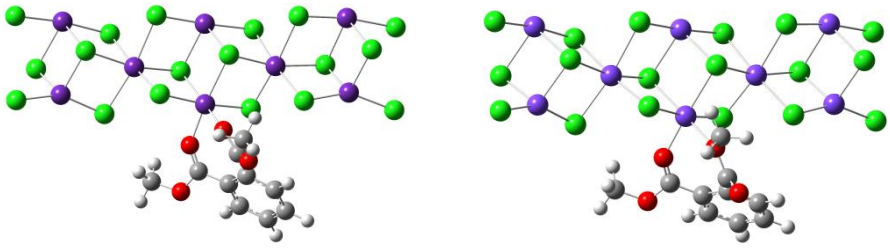

Clu_110_27 / DMP-**B** Clu_110_27 / DMP-**A**

Figure 3.7 Adducts of DMP-**B** and DMP-**A** with Clu_110_27 (i.e. on a $MgCl_2$(110)-like edge). Corresponding binding energies are reported in **Table 3.4**, entries **2** and **1** respectively.

Table 3.4 Binding energies of different conformers of DMP on Clu_110_27 (i.e. on $MgCl_2$(110)-like edges) and Clu_104_24 (i.e. on $MgCl_2$(104)-like edges).

Entry	Structure	ΔH_{ads} [kcal/mol]	ΔG_{ads} [kcal/mol]	Binding mode
1	Clu_110_27 / DMP-**A**	-33.7	-19.7	Chelating
2	Clu_110_27 / DMP-**B**	-41.5	-27.8	Chelating
3	Clu_110_27 / DMP-**A**	-27.2	-16.0	Monodentate
4	Clu_110_27 / DMP-**B**[a]	-36.3	-20.6	Bridging
5	Clu_110_27 / DMP-**B**[a]	-38.5	-23.3	Bridging
6	Clu_104_24 / DMP-**A**	-25.3	-13.6	Monodentate
7	Clu_104_24 / DMP-**B**[a]	-37.8	-23.2	Bridging
8	Clu_104_24 / DMP-**B**[a]	-38.9	-24.2	Bridging

[a] Different adsorbate orientations with respect to the cluster edge.

With Clu_104_24, in turn, i.e. a $MgCl_2$(104)-like edge, DMP-**B** yielded two adducts with similar binding energy (entries **7** and **8** of **Table 3.4**), in which the donor bridged two 5-coordinated Mg atoms using both carbonyl O (**Figure 3.8**). DMP-**A**, instead, could only bind in monodentate fashion using one carbonyl O, once again mimicking a monoester (entry **6** of **Table 3.4**).

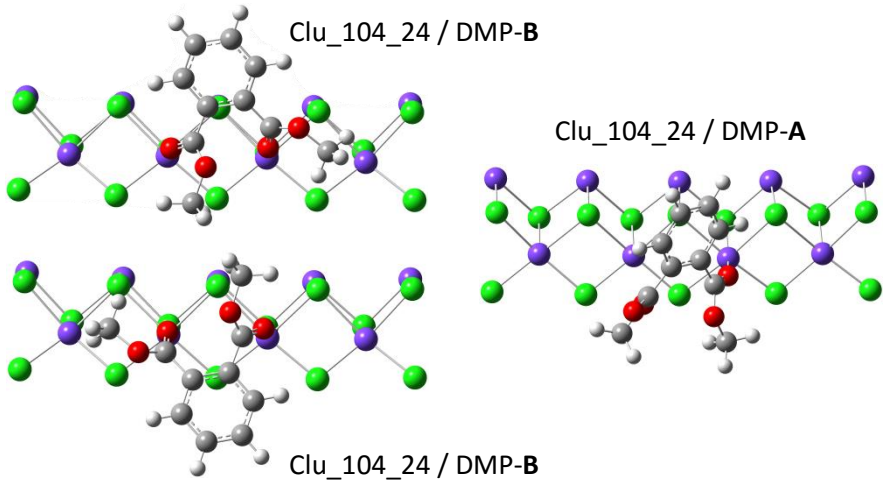

Figure 3.8 Adducts of DMP with Clu_104_24 (i.e. a $MgCl_2$(104)-like edge). For corresponding binding energies see **Table 3.4**.

Overall, the results of **Table 3.4** indicate that DMP can bind similarly well to $MgCl_2$(104)-like and $MgCl_2$(110)-like edges (albeit with different adsorption modes); this is consistent with qualitative hypotheses in the previous literature.[5, 12]

3.2.3.2 DMSuc adsorption modes

The computational evaluation of DMSuc adsorption on Clu_110_27 (i.e. $MgCl_2$(110)-like edges) led us to conclude that this ID can bind in chelating as well as bridging fashion, provided that steric repulsions of the ester groups with the surface are not too severe (**Table 3.5**). In particular,

the lower binding energies calculated for entries **1**, **5** and **7** can be traced to repulsions between methyl groups and Cl atoms next to the binding sites (**Figure 3.9**). In turn, this suggests that succinates with bulkier alkyl fragments may behave rather differently.[13] For conformer DMSuc-**M3** (entry **6** of **Table 3.5**), chelation involved one carbonyl and one ether O (**Figure 3.9**), which resulted into a much lower binding energy compared with chelation using two carbonyl groups.

Table 3.5 Binding energies of different conformers of DMSuc on Clu_110-27 (i.e. a $MgCl_2$(110)-like edge).

Entry	Structure	ΔH_{ads} [kcal/mol]	ΔG_{ads} [kcal/mol]	Binding mode
1	Clu_110_27 / DMSuc-**M1**	-41.2	-25.7	Bridging
2	Clu_110_27 / DMSuc-**M1**	-43.3	-28.7	Chelating
3	Clu_110_27 / DMSuc-**M2**	-43.5	-29.7	Bridging
4	Clu_110_27 / DMSuc-**M2**	-41.3	-25.6	Chelating
5	Clu_110_27 / DMSuc-**M3**	-41.6	-24.9	Bridging
6	Clu_110_27 / DMSuc-**M3**	-35.8	-21.4	Chelating
7	Clu_110_27 / DMSuc-**R1**	-37.9	-22.9	Bridging
8	Clu_110_27 / DMSuc-**R1**	-44.5	-30.3	Chelating
9	Clu_110_27 / DMSuc-**R2**[a]	-44.3	-28.5	Bridging
10	Clu_110_27 / DMSuc-**R2**[a]	-42.0	-28.1	Chelating
11	Clu_110_27 / DMSuc-**R2**[a]	-43.3	-28.4	Bridging
12	Clu_110_27 / DMSuc-**R2**[a]	-28.4	-16.3	Monodentate
13	Clu_110_27 / DMSuc-**R3**	-43.8	-28.2	Bridging
14	Clu_110_27 / DMSuc-**R3**	-42.8	-28.8	Chelating
15	Clu_110_27 / DMSuc-**S2**	-40.5	-27.0	Bridging
16	Clu_110_27 / DMSuc-**S2**	-41.1	-27.8	Chelating

[a] Different adsorbate orientations with respect to the cluster edge.

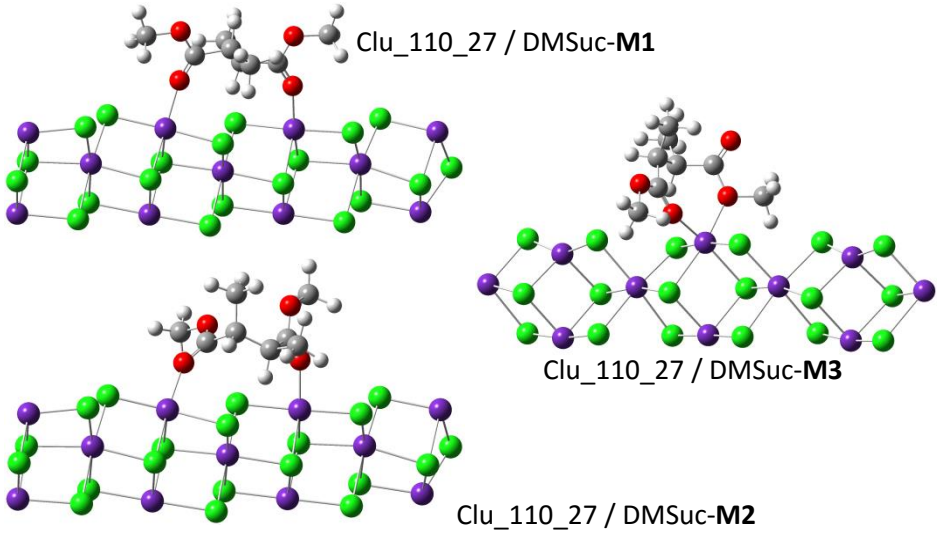

Figure 3.9 Adducts of DMSuc with Clu_110_27 (i.e. a $MgCl_2$(110)-like edge). Corresponding binding energies are reported in **Table 3.5**.

Concerning adsorption on Clu_104_24 (i.e. a $MgCl_2$(104)-like edge), the bridging mode turned out to be favored over the monodentate one (which is energetically similar to a monoester molecule), and binding energies to be independent of the orientation of the donor with respect to the edge (**Table 3.6**).

Overall, our conclusion is that R and S enantiomers of DMSuc do not discriminate between binding to 4-coordinated and 5-coordinated Mg sites. The meso form, instead, has a slight preference for 4-coordinated Mg sites.

Table 3.6 Binding energies of different conformers of DMSuc on Clu_104_24 (i.e. a $MgCl_2$(104)-like edge).

Entry	Structure	ΔH_{ads} [kcal/mol]	ΔG_{ads} [kcal/mol]	Binding mode
1	Clu_104_24 / DMSuc-**M1**[a]	-35.1	-19.7	Bridging
2	Clu_104_24 / DMSuc-**M1**[a]	-35.2	-19.9	Bridging
3	Clu_104_24 / DMSuc-**M2**	-37.0	-21.7	Bridging
4	Clu_104_24 / DMSuc-**M3**	-37.1	-21.6	Bridging
5	Clu_104_24 / DMSuc-**R1**	-36.9	-21.7	Bridging
6	Clu_104_24 / DMSuc-**R2**[a]	-39.3	-24.3	Bridging
7	Clu_104_24 / DMSuc-**R2**[a]	-39.7	-25.3	Bridging
8	Clu_104_24 / DMSuc-**R2**[a]	-24.5	-11.9	Monodentate
9	Clu_104_24 / DMSuc-**R2**[a]	-26.0	-13.9	Monodentate
10	Clu_104_24 / DMSuc-**R3**	-38.0	-23.6	Bridging
11	Clu_104_24 / DMSuc-**S2**	-34.4	-18.7	Bridging
12	Clu_104_24 / DMSuc-**S3**	-39.6	-25.5	Bridging

[a] Different adsorbate orientations with respect to the cluster edge.

3.2.4 1,3-dimethoxypropane IDs

In the 1990s, a 5th-generation of ZNC was introduced featuring 2,2-dialkyl-1,3-dimethoxypropane IDs. Notably, they represent the first and – at the present stage – the only case among $MgCl_2$-supported systems in which the addition of an ED is not mandatory to achieve a high stereoselectivity in propene polymerization.[14] This has been traced to the fact that IDs belonging in this class do not react with the R_3Al co-catalyst, and therefore are not extracted from the solid phase during polymerization. Another peculiarity is the comparatively low polydispersity of the polymer obtained, which was explained in terms of a pseudo-single-center behavior, traceable in turn for the strong preference of these IDs for

adsorption on 4-coordinated Mg (i.e. $MgCl_2$(110)-like crystal edges).[4a, 15]

As a prototype, we investigated 2,2-dimethyl-1,3-dimethoxy-propane (DMMP). We are aware that the steric demand of this molecule is not large enough to ensure an effective catalyst modification; as a matter of fact, industrially relevant molecules bear two bulky alkyl fragments at C-2.[4c, 16] On the other hand, for an extensive computational screening, DMMP is already a challenging structure, due to the high conformational flexibility; we are confident that our conclusions can be extended to bulkier homologues.

In agreement with the previous literature,[4a, 6b] our conformational analysis identified four structures differing in the orientation of the methoxy groups around the propane chain (**Figure 3.10**). Three of them showed electronic energy values very close to each other (differences within 1.5 kcal/mol), whereas one (DMMP-**B**) was ~3.5 kcal/mol higher. Preliminary studies on other 2,2-dialkyl-1,3-dimethoxypropanes with larger substituents gave very similar results (i.e. energy differences below 5 kcal/mol). All four conformers were retained for the adsorption study.

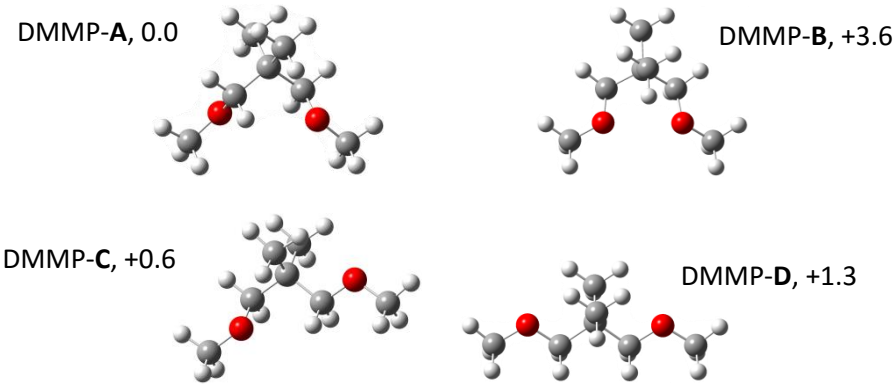

Figure 3.10 Different DMMP conformers with relative electronic energy values (in kcal/mol).

On inspection, only DMMP-**A** and DMMP-**B** are suited to chelate 4-coordinated Mg atoms on $MgCl_2$(110)-like edges; the optimized structures for Clu_110_27 (**Figure 3.11**) confirmed this educated guess. This binding mode turned out to be favored by more than 10 kcal/mol over monodentate adsorption for DMMP-**C** and DMMP-**D** (**Table 3.7**).

Similarly, in the case of $MgCl_2$(104)-like edges, the bridging mode, also possible for DMMP-**A** and DMMP-**B** only, was calculated to be stronger by at least 10 kcal/mol than the monodentate modes (entries **6-8** of **Table 3.7**).

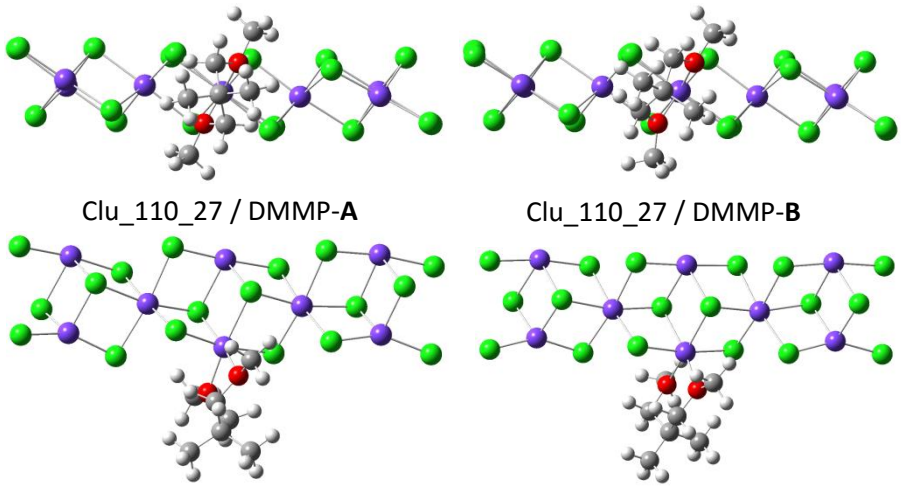

Figure 3.11 Different views of the chelating adsorption of DMMP-**A** and DMMP-**B** on Clu_110_27 (i.e. a MgCl2(110)-like edge)**.**

Overall, based on the results of **Table 3.7**, we can conclude that the literature claim of a strong preference of this ID class for adsorption on 4-coordinate Mg is fully justified.[3b, 4]

Table 3.7 Binding energies of different conformers of DMMP on Clu_110_27 (i.e. a $MgCl_2$(110)-like edge) and Clu_104_24 (i.e. a $MgCl_2$(104)-like edge).

Entry	Structure	ΔH_{ads} [kcal/mol]	ΔG_{ads} [kcal/mol]	Binding mode
1	Clu_110_27 / DMMP-**A**	-39.4	-26.0	Chelating
2	Clu_110_27 / DMMP-**B**	-43.5	-29.4	Chelating
3	Clu_110_27 / DMMP-**B**	-29.1	-14.6	Bridging
4	Clu_110_27 / DMMP-**C**	-27.1	-14.4	Monodentate
5	Clu_110_27 / DMMP-**D**	-26.6	-14.9	Monodentate
6	Clu_104_24 / DMMP-**A**	-32.2	-16.4	Monodentate
7	Clu_104_24 / DMMP-**B**[a]	-32.6	-17.3	Bridging
8	Clu_104_24 / DMMP-**B**[a]	-34.9	-19.2	Bridging

[a] Different adsorbate orientations with respect to the cluster edge.

3.2.5 Dialkoxysilane EDs

In **Chapter 1** and previous sections of the present one, we recalled that the vast majority of $MgCl_2$-supported ZNC formulations include a so-called External Donor (ED), which is added along with the R_3Al co-catalyst. In general (generic) terms, the ED integrates the action of the ID, ending up with a more stereoselective catalyst.[16] From a mechanistic standpoint, it has been suggested that ED molecules poison catalytic species of low(er) stereoselectivity, and/or change them into (more) stereoselective ones.[1b, 17] The latter hypothesis is more plausible in case the ID reacts with the R_3Al and is extracted from the solid phase during polymerization; as a matter of fact, experimental evidence of an extensive ID/ED exchange has been reported.[1c]

With the only exception of 3rd-generation catalysts (section 3.2.2), in which both the ID and the ED are aromatic monoesters, the ED is an alkoxysilane of general formula $R_xSi(OR^I)_{4-x}$, where R = alkyl or aryl, R^I = methyl or ethyl, and x = 1 or 2.[18]

As a prototype, we investigated the adsorption of dimethyldimethoxysilane (DMMSi). For this molecule, we identified two conformers that differ for the relative orientations of the methoxy groups and feature similar values of electronic energy (**Figure 3.12**). A third structure, namely DMMSi-**C**, could be obtained only as an adsorbate on a $MgCl_2$ edge; in vacuum the conformer is poorly stable, probably due to steric repulsions between the methyl groups, which are really close to each other.

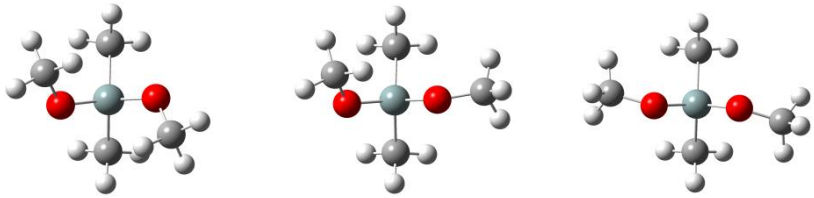

DMMSi-**A**, 0.0 DMMSi-**B**, +1.3 DMMSi-**C**, —

Figure 3.12 Different DMMSi conformers with relative electronic energy (in kcal/mol).

The calculated values of binding energy to Clu_110_27 and Clu_104_24, summarized in **Table 3.8**, indicate a moderate preference of DMMSi to chelate 4-coordinated Mg atoms, in line with experimental observations.[18] This binding mode was only obtained with the donor in **C** conformation (which is indeed the only one orienting both O atoms towards the edge). The bridging mode, in turn, turned out to be feasible on

$MgCl_2$(104)-like edges only, and its binding energy was calculated to be comparable with that for monodentate binding on 4-coordinated Mg. On $MgCl_2$(110)-like edges, the bridging interaction is strongly disfavored because the distance between the two O atoms is too small (**Figure 3.13**).[3b]

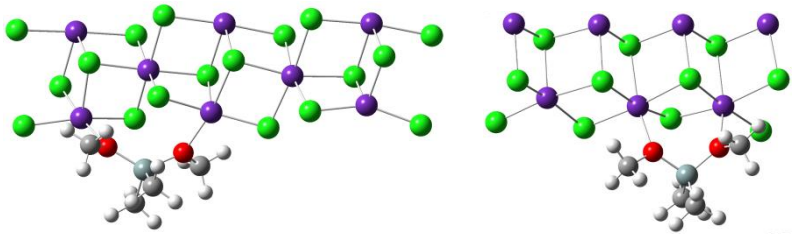

Figure 3.13 Calculated structures of bridging DMMSi adsorption on $MgCl_2$(110)-like and $MgCl_2$(104)-like edges. The former was found to be unstable.

Table 3.8 Binding energies of different conformers of DMMSi on Clu_110_27 (i.e. a $MgCl_2$(110)-like edge) and Clu_104_24 (i.e. a $MgCl_2$(104)-like edge).

Entry	Structure	ΔH_{ads} [kcal/mol]	ΔG_{ads} [kcal/mol]	Binding mode
1	Clu_110_27 / DMMSi-**B**	-24.6	-13.4	Monodentate
2	Clu_110_27 / DMMSi-**C**	-35.6	-23.1	Chelateing
3	Clu_104_24 / DMMSi-**A**[a]	-21.3	-7.6	Monodentate
4	Clu_104_24 / DMMSi-**A**[a]	-20.8	-7.1	Monodentate
5	Clu_104_24 / DMMSi-**B**[a]	-30.4	-15.1	Bridging
6	Clu_104_24 / DMMSi-**B**[a]	-29.4	-12.7	Bridging
7	Clu_104_24 / DMMSi-**C**[a]	-30.1	-13.9	Bridging
8	Clu_104_24 / DMMSi-**C**[a]	-29.3	-13.0	Bridging

[a] Different adsorbate orientations with respect to the cluster edge.

In general terms, the calculated values of adsorption enthalpy and Gibbs Free Energy are appreciably lower than those for typical bidentate IDs; this is consistent with the experimental fact that alkoxysilane EDs adsorb extensively on the solid catalyst phase only in case the ID is reactive with R_3Al.

References

1. (a) Goodall, B. L., *J. Chem. Educ.* **1986,** *63* (3), 191; (b) Chadwick, J. C.; Morini, G.; Balbontin, G.; Camurati, I.; Heere, J. J. R.; Mingozzi, I.; Testoni, F., *Macromol. Chem. Phys.* **2001,** *202* (10), 1995-2002; (c) Moore, E. P., Jr., Ed., *Polypropylene Handbook: Polymerization, Characterization, Properties, Processing, Applications*. Hanser Publishers: Munich, Germany: 1996.
2. Cecchin, G.; Morini, G.; Piemontesi, F., Ziegler-Natta Catalysts. In *Kirk-Othmer Encyclopedia of Chemical Technology*, John Wiley & Sons, Inc.: 2000.
3. (a) Taniike, T.; Terano, M., *Macromol. Rapid Commun.* **2007,** *28* (18-19), 1918-1922; (b) Correa, A.; Piemontesi, F.; Morini, G.; Cavallo, L., *Macromolecules* **2007,** *40* (25), 9181-9189; (c) Corradini, P.; Busico, V.; Cavallo, L.; Guerra, G.; Vacatello, M.; Venditto, V., *J. Mol. Catal.* **1992,** *74* (1–3), 433-442.
4. (a) Toto, M.; Morini, G.; Guerra, G.; Corradini, P.; Cavallo, L., *Macromolecules* **2000,** *33* (4), 1134-1140; (b) Brambilla, L.; Zerbi, G.; Piemontesi, F.; Nascetti, S.; Morini, G., *J. Phys. Chem. C* **2010,** *114* (26), 11475-11484; (c) Potapov, A. G.; Politanskaya, L. V., *J. Mol. Catal. A: Chem.* **2013,** *368–369* (0), 159-162.
5. Song, B. G.; Ihm, S.-K., *J. Appl. Polym. Sci.* **2014,** *131* (15), n/a-n/a.
6. (a) Taniike, T.; Terano, M., *J. Catal.* **2012,** *293* (0), 39-50; (b) Lee, J. W.; Jo, W. H., *J. Organomet. Chem.* **2009,** *694* (19), 3076-3083; (c) Stukalov, D. V.; Zakharov, V. A.; Zilberberg, I. L., *J. Phys. Chem. C* **2009,** *114* (1), 429-435.
7. (a) Liu, B.; Cheng, R.; Liu, Z.; Qiu, P.; Zhang, S.; Taniike, T.; Terano, M.; Tashino, K.; Fujita, T., *Macromol. Symp.* **2007,** *260* (1), 42-48; (b) Morini, G.; Albizzati, E.; Balbontin, G.; Mingozzi, I.; Sacchi, M. C.; Forlini, F.; Tritto, I., *Macromolecules* **1996,** *29* (18), 5770-5776.
8. (a) Sormunen, P.; Hjertberg, T.; Iiskola, E., *Die Makromolekulare Chemie* **1990,** *191* (11), 2663-2673; (b) Stukalov, D. V.; Zakharov, V. A.; Potapov, A. G.; Bukatov, G. D., *J. Catal.* **2009,** *266* (1), 39-49; (c) Chien, J. C. W.; Dickinson, L. C.; Vizzini, J., *J. Polym. Sci., Part A: Polym. Chem.* **1990,** *28* (9), 2321-2333.
9. (a) Solanko, K. A.; Bond, A. D., *Acta Crystallographica Section B*

2011, *67* (5), 437-445; (b) Wang, R.; Dols, T. S.; Lehmann, C. W.; Englert, U., *Z. Anorg. Allg. Chem.* **2013,** *639* (11), 1933-1939.

10. Parodi, S.; Nocci, R.; Giannini, U.; Barbe, P. C.; Scata, U. Components and catalysts for the polymerization of olefins. EP45977A2, 1982.

11. Kminsky, W., *Polyolefines: 50 years after Ziegler and Natta I*. 1 ed.; Springer-Varlag Berlin Heidelberg: Berlin, 2013; Vol. 257, p 257.

12. (a) Cheruvathur, A. V.; Langner, E. H. G.; Niemantsverdriet, J. W.; Thüne, P. C., *Langmuir* **2012,** *28* (5), 2643-2651; (b) Andoni, A.; Chadwick, J. C.; Niemantsverdriet, H. J. W.; Thüne, P. C., *J. Catal.* **2008,** *257* (1), 81-86.

13. (a) Jiang, X.; Chen, Y.-p.; Fan, Z.-q.; Wang, Q.; Fu, Z.-s.; Xu, J.-t., *J. Mol. Catal. A: Chem.* **2005,** *235* (1–2), 209-219; (b) Wen, X.; Ji, M.; Yi, Q.; Niu, H.; Dong, J.-Y., *J. Appl. Polym. Sci.* **2010,** *118* (3), 1853-1858.

14. Albizzati, E.; Barbe, P. C.; Noristi, L.; Scordamaglia, R.; Barino, L.; Giannini, U.; Morini, G. Electron-donor compound-titanium catalysts for the polymerization of olefins. EP361494A2, 1990.

15. (a) Albizzati, E.; Giannini, U.; Morini, G.; Galimberti, M.; Barino, L.; Scordamaglia, R., *Macromol. Symp.* **1995,** *89* (1), 73-89; (b) Barino, L.; Scordamaglia, R., *Macromol. Symp.* **1995,** *89* (1), 101-111.

16. Sacchi, M. C.; Forlini, F.; Tritto, I.; Locatelli, P.; Morini, G.; Noristi, L.; Albizzati, E., *Macromolecules* **1996,** *29* (10), 3341-3345.

17. Barbè, P. C.; Noristi, L.; Baruzzi, G., *Die Makromolekulare Chemie* **1992,** *193* (1), 229-241.

18. Busico, V.; Causà, M.; Cipullo, R.; Credendino, R.; Cutillo, F.; Friederichs, N.; Lamanna, R.; Segre, A.; Van Axel Castelli, V., *J. Phys. Chem. C* **2008,** *112* (4), 1081-1089.

Chapter 4. Adsorption of $TiCl_4$

4.1 Experimental and computational background

In the vast majority of cases, $TiCl_4$ is the precursor of the catalytic species in $MgCl_2$-supported ZNCs. In **Chapter 1**, we have discussed typical formulations and pre-catalyst preparation routes. In particular, we noted that, in present day controlled morphology catalysts, $TiCl_4$ is also used as a chlorinating agent to precipitate nano-structured $MgCl_2$ from a soluble or low-melting precursor in the presence of an ID;[1] this step is characterized by rather harsh conditions (i.e. repeated treatments with liquid or concentrated $TiCl_4$ for several hours at high (>150°C) temperature, followed by an extensive hydrocarbon hot washing). In typical cases, the resulting pre-catalytic solids consist of highly disordered $MgCl_2$, 10 ÷ 20 wt-% ID, and 5 ÷ 15 wt-% $TiCl_4$; it is generally believed that the latter two constituents are independently chemisorbed on the lateral terminations of $MgCl_2$ crystallites.

In the same **Chapter 1** we recalled that, at the end of the 1970s, Giannini et al.[2] and Corradini et al.[3] proposed that $TiCl_4$ adsorbs epitaxially on $MgCl_2$(100) [$MgCl_2$(104) for α-$MgCl_2$] and $MgCl_2$(110) surfaces. According to Corradini,[3] who was the first to apply Molecular Mechanics to evaluate the enantioselectivity of propene insertion at computational models of Ziegler-Natta active sites, dinuclear Ti_2Cl_8 adducts on $MgCl_2$(104) would be precursors to isotactic-selective catalytic species, whereas

mononuclear $TiCl_4$ adducts on $MgCl_2$(104) and $MgCl_2$(110) would give rise to undesired poorly stereoselective species. Strong chemisorption of the ID on $MgCl_2$(110) was proposed to hamper the weaker $TiCl_4$ binding to the same edges, thus enhancing catalyst stereoselectivity.[4] For many years this interpretation was widely endorsed, and the disclosure in the mid-1990s of 1,3-dimethoxypropanes as 'design' IDs for the chelation of 4-coordinated Mg was interpreted as a crucial experimental demonstration.[5]

It came therefore by surprise that, in the late 1990s, new experimental and computational evidences in conflict with Corradini's view were reported. As a matter of fact, combined TREF/^{13}C NMR analyses of polymer microstructure demonstrated that the chemical structures of the used ID and ED have a direct impact on PP stereoregularity;[6] moving from this fact, Busico et al.[6-7] introduced a novel active site model in which LB molecules at non-bonded contact modulate the catalytic pocket similarly to the ancillary ligand(s) of molecular catalysts, and demonstrated that epitaxial mononuclear isotactic-selective species may well be located on $MgCl_2$(110) terminations. More or less at the same time, the first quantitative DFT calculations by Ziegler[8] concluded that $TiCl_4$ binding to $MgCl_2$ is very weak, and all epitaxial models proposed that far would be unstable. Much more recently, Busico and Causà[9] demonstrated that Ziegler's claims were too extreme, because $TiCl_4$ adsorption on $MgCl_2$ is largely dispersion-driven, and a DFT-D approach is mandatory for a realistic evaluation of the system; in a seminal paper,[10] results of periodic DFT-D calculations were reported indicating that the epitaxial adsorption of single

$TiCl_4$ units on $MgCl_2$(110) crystal terminations is feasible, albeit with moderate strength (ΔG_{ads} ~ -10 kcal/mol), and should be regarded as the most plausible precursors to Ziegler-Natta catalytic species.

4.2 Computational study of $TiCl_4$ adsorption on $MgCl_2$ clusters

4.2.1 Adsorption on $MgCl_2$(104)-like and $MgCl_2$(110)-like surfaces

In the first part of our investigation, we evaluated the conclusions of the aforementioned Periodic DFT-D calculations by Busico and Causà[10] in the framework of our Cluster Approach. For this, we utilized the same model clusters adopted to study ID and ED adsorption, namely Clu_104_24 and Clu_110_27 (**Chapter 3**). For the former, we found it necessary to stabilize the corners by means of H_2O adsorption (see **Chapter 2**), in order to avoid the problem of multiple minima due to adsorption-induced cluster reconstructions.

For each cluster, we considered Corradini's epitaxial adducts (mononuclear and, when possible, dinuclear), as well as some non-epitaxial ones also proposed in the previous literature (e.g. Parrinello[11] and Edge[12] models). The results of our calculations are summarized in **Table 4.1**, whereas the optimized structures are shown in **Figure 4.1** (for Clu_110_27) and **Figure 4.2** (for Cluster Clu_104_24).

Table 4.1 Binding energies of several Ti_xCl_{4x} species on Clu_110_27 and Clu_104_24 (**Figures 4.1** and **4.2**). Corresponding results of Periodic DFT-D calculations[10] are also reported (parentheses brackets) where available.

Entry	Structure	ΔH_{ads} [kcal/mol]	ΔG_{ads} [kcal/mol]	Model
1	Clu_110_27 / $TiCl_4$ -**A**	-21.9	-6.4 (-10.3)	Corradini
2	Clu_110_27 / $TiCl_4$ -**B**	-8.3	+3.9	Parrinello
3	Clu_110_27 / $TiCl_4$ -**C**	-8.1	+2.4	Edge
4	Clu_104_24 / $TiCl_4$ -**A**	-9.4	+2.0 (+1.3)	Corradini
4[I]	Clu_104_24 / $TiCl_4$ -**A**[I]	-10.9	+2.2	
5	Clu_104_24 / Ti_2Cl_8 -**B**	-16.2	-1.1	Corradini
5[I]	Clu_104_24 / Ti_2Cl_8 -**B**[I]	-10.5	+3.5 (+2.3)	

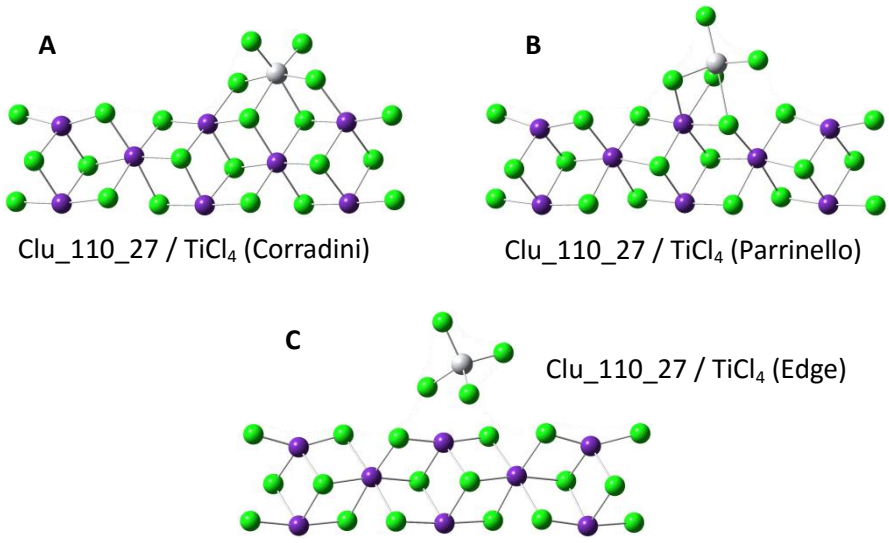

Figure 4.1 Local structures of various Clu_110_27 / $TiCl_4$ adducts.

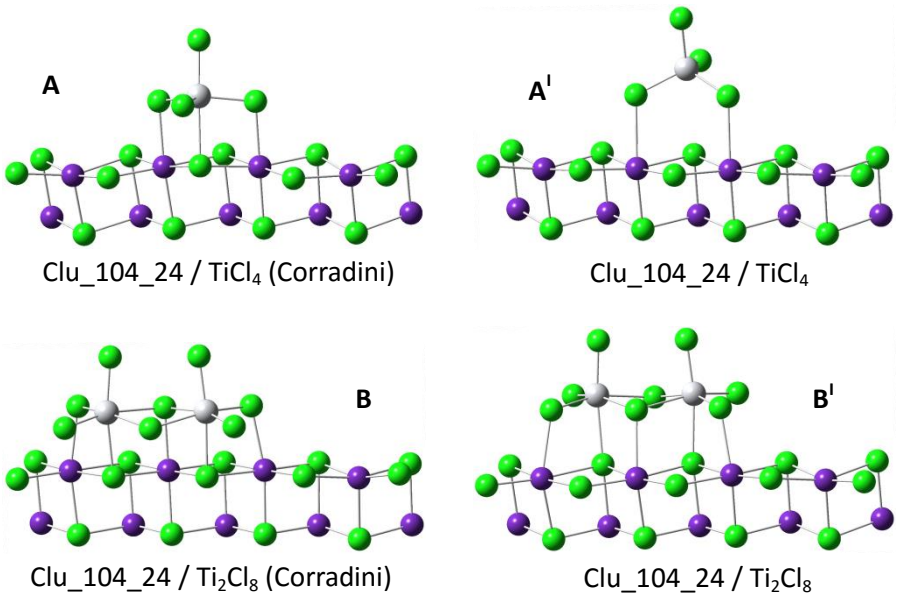

Figure 4.2 Local structures of various Clu_104_24 / Ti_nCl_{4n} adducts.

The following points should be noted:

(a) of all investigated adducts (including epitaxial and non-epitaxial structures), the only case of chemisorption (as showing a patently negative value of ΔG_{ads}) corresponds to a mononuclear epitaxial $TiCl_4$ unit bound to a $MgCl_2$(110)-like edge; this is in full agreement with the conclusions of the Periodic DFT-D investigation of ref 10. All other cases can be described, at most, in terms of physisorption;

(b) in general, the cluster DFT-D results are in remarkably good agreement with periodic DFT-D ones when available;

(c) the values of Gibbs free energies in **Table 4.1** are indicative of a fairly large entropic penalty whenever the binding mode is

associated with a major rearrangement of Ti geometry from originally tetrahedral to trigonal bipyramidal or octahedral; this is probably due to the loss of many vibrational and rotational degrees of freedom. This certainly represents one reason for the poor binding.

4.2.2 Adsorption on 'defective' $MgCl_2$ clusters

$MgCl_2$ primary particles in real-world ZNCs are very small and highly defective. Defects can impact on adsorption modes and strengths, particularly in case of rather poor adsorbates such as $TiCl_4$. In view of this, and taking advantage from the superior versatility of the Cluster Approach compared with a periodic one, we extended our investigation to specific defect-containing clusters.

Only few computational studies on this subject have been published so far.[13] Cavallo and coworkers[13a] reported that removing one single $MgCl_2$ unit located on the corner of two well-formed $MgCl_2$(104) edges, thus generating two 4-coordinated Mg atoms, is an energetically feasible process. Plausibly, Pakkanen[13c] and Cavallo[13e] concluded that the relative stability of these kind of defective structures is intermediate between those of 'ideal' $MgCl_2$(104) and $MgCl_2$(110) surfaces, confirming once again the feasibility of such a formation process.

We examined in depth hole-type and a step-type defects, as shown in **Figure 4.3**. In the former case, one single $MgCl_2$ unit was removed from the middle of a finite $MgCl_2$(110)-like edge; in the latter, instead, a few consecutive $MgCl_2$ units were stripped from a finite $MgCl_2$(104)-like or

$MgCl_2$(110)-like edge. Of course, these operations generated Mg centers with a different coordination compared with the unperturbed edge. In both cases, we then evaluated the optimized structures resulting from the epitaxial adsorption of a single $TiCl_4$ unit at the defect (as shown in the same **Figure 4.3**); the results are reported in **Chart 4.1**, comparatively with those for adsorption on an unperturbed $MgCl_2$(110)-like edge.

Step_104_18 / $TiCl_4$

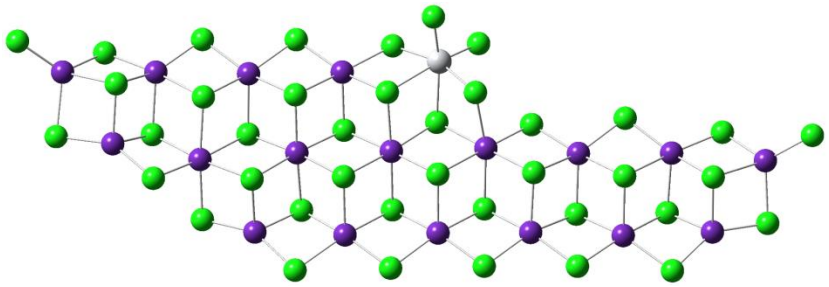

Step_110_19 / $TiCl_4$

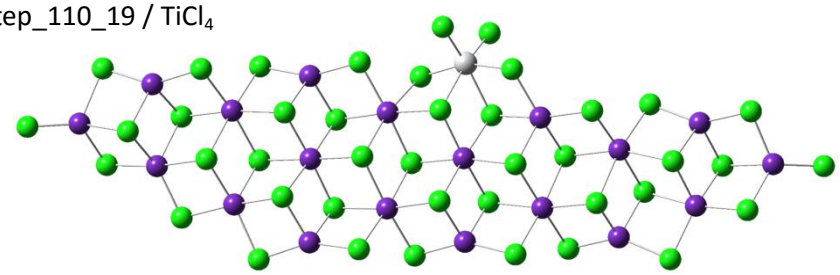

Hole_110_22 / $TiCl_4$

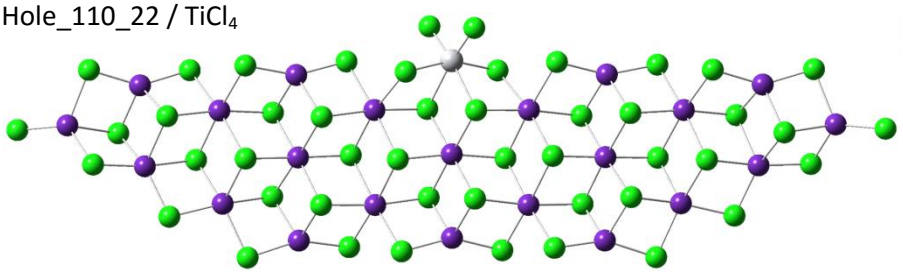

Figure 4.3 Adducts of $TiCl_4$ (in Corradini's mode) on 'defective' $MgCl_2$ clusters (see text).

Chart 4.1 Values of adsorption enthalpy (black) and Gibbs free energy (red) for a single epitaxial $TiCl_4$ unit at the defective locations of **Figure 4.3**, compared with the corresponding values for an unperturbed $MgCl_2$(110)-like edge.

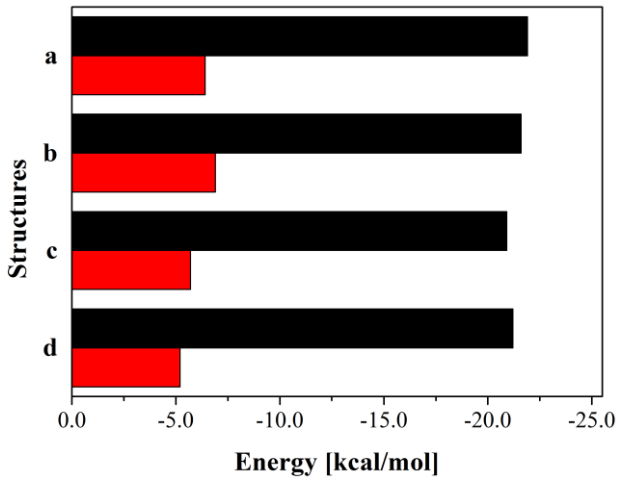

Legenda: **a** = unperturbed $MgCl_2$(110)-like edge (i.e. Clu_110_27); **b** = step-type 104_18; **c** = step-type 110_19; **d** = hole-type 110_22 (**Figure 4.3**).

It is important to note that all values in **Chart 4.1** are very close to each other. This suggests that the epitaxial chemisorption of mononuclear $TiCl_4$ is governed by the local environment at the adsorption site, irrespective of whether this is located on an 'ideal' or a defective edge. Very recent independent results by Cavallo led to the same conclusion.[13e]

References

1. (a) Huang, R.; Malizia, F.; Pennini, G.; Koning, C. E.; Chadwick, J. C., *Macromol. Rapid Commun.* **2008,** *29* (21), 1732-1738; (b) Malizia, F.; Fait, A.; Cruciani, G., *Chemistry – A European Journal* **2011,** *17* (49), 13892-13897; (c) Bart, J. C. J.; Roovers, W., *JOURNAL OF MATERIALS SCIENCE* **1995,** *30* (11), 2809-2820; (d) Forte, M. C.; Coutinho, F. M. B., *Eur. Polym. J.* **1996,** *32* (2), 223-231; (e) Buchacher, P.; Fischer, W.; Aichholzer, K. D.; Stelzer, F., *J. Mol. Catal. A: Chem.* **1997,** *115* (1), 163-171; (f) Stukalov, D. V.; Zakharov, V. A.; Potapov, A. G.; Bukatov, G. D., *J. Catal.* **2009,** *266* (1), 39-49.
2. Giannini, U., *Die Makromolekulare Chemie* **1981,** *5* (S19811), 216-229.
3. Corradini, P.; Barone, V.; Fusco, R.; Guerra, G., *Gazz. Chim. Ital.* **1983,** *113* (9-10), 601-7.
4. Busico, V.; Corradini, P.; De Martino, L.; Proto, A.; Savino, V.; Albizzati, E., *Die Makromolekulare Chemie* **1985,** *186* (6), 1279-1288.
5. (a) Scordamaglia, R.; Barino, L., *Macromol. Theory Simul.* **1998,** *7* (4), 399-405; (b) Albizzati, E.; Giannini, U.; Morini, G.; Galimberti, M.; Barino, L.; Scordamaglia, R., *Macromol. Symp.* **1995,** *89* (1), 73-89.
6. Busico, V.; Cipullo, R.; Monaco, G.; Talarico, G.; Vacatello, M.; Chadwick, J. C.; Segre, A. L.; Sudmeijer, O., *Macromolecules* **1999,** *32* (13), 4173-4182.
7. Corradini, P.; Guerra, G.; Cavallo, L., *Acc. Chem. Res.* **2004,** *37* (4), 231-241.
8. Seth, M.; Margl, P. M.; Ziegler, T., *Macromolecules* **2002,** *35* (20), 7815-7829.
9. Credendino, R.; Busico, V.; Causa, M.; Barone, V.; Budzelaar, P. H. M.; Zicovich-Wilson, C., *PCCP* **2009,** *11* (30), 6525-6532.
10. D'Amore, M.; Credendino, R.; Budzelaar, P. H. M.; Causá, M.; Busico, V., *J. Catal.* **2012,** *286* (0), 103-110.
11. Boero, M.; Parrinello, M.; Terakura, K., *J. Am. Chem. Soc.* **1998,** *120* (12), 2746-2752.
12. Monaco, G.; Toto, M.; Guerra, G.; Corradini, P.; Cavallo, L., *Macromolecules* **2000,** *33* (24), 8953-8962.
13. (a) Correa, A.; Credendino, R.; Pater, J. T. M.; Morini, G.; Cavallo, L., *Macromolecules* **2012,** *45* (9), 3695-3701; (b) Bazhenov, A.; Linnolahti, M.;

Karttunen, A. J.; Pakkanen, T. A.; Denifl, P.; Leinonen, T., *J. Phys. Chem. C* **2012,** *116* (14), 7957-7961; (c) Bazhenov, A.; Linnolahti, M.; Pakkanen, T. A.; Denifl, P.; Leinonen, T., *J. Phys. Chem. C* **2014,** *118* (9), 4791-4796; (d) Kuklin, M. S.; Bazhenov, A. S.; Denifl, P.; Leinonen, T.; Linnolahti, M.; Pakkanen, T. A., *Surf. Sci.* **2015,** *635* (0), 5-10; (e) Credendino, R.; Liguori, D.; Fan, Z.; Morini, G.; Cavallo, L., *ACS Catalysis* **2015,** *5* (9), 5431-5435.

Chapter 5. Towards real active site models

5.1 Research of meaningful ternary systems

5.1.1 Brief historical introduction

ZNCs constitute an industrial and academic research area of extreme complexity. Arriving at an atomic-level understanding of the nature of the active sites, and the mechanisms that control the experimental behavior of these systems would represent a remarkable success. It would open the way rational tuning of catalyst properties to produce the most suitable material for each industrial application.

In view of the difficulties associated with experimental characterization of ZNCs, several groups have used computational approaches instead of, or in addition to, physicochemical methods.

The first computational studies[1] in this field used a combination of QM and MM techniques on very small systems in order to evaluate catalytic properties of different Ti(III) models. Although the results of such studies cannot be considered definitive, they clearly indicated that Lewis bases (ID and/or ED) are essential for obtaining highly selective active sites.

DFT simulations of more complex models[2] started to appear in the literature only during the last 10 years. These confirmed the inadequacy of the binary $MgCl_2/TiCl_4$ system to generate isospecific centers. Moreover, also ternary $MgCl_2/TiCl_4$/donor models on edges exposing only 4-coordinated Mg sites resulted in poor isoselectivity because of the long distance between the adsorption sites of the donor molecules and the

active Ti species. The combination of these results, with the finding that $TiCl_4$ only binds to $MgCl_2$(110)-like lateral terminations, led to the hypothesis that highly regio- and stereospecific active sites should be located primarily on defects of support nano-particles.[3] However, only few specific type of model sites could be proposed based on this hypothesis.

Fully relaxed models with dimensions close to those of real-life catalyst primary particles have been never adopted, so it remains unclear how close to reality present-day computer simulations are. With this in mind, we began a re-examination of the formation of a supported pre-catalyst, using at first small models to identify all meaningful types of sites, and then $MgCl_2$ clusters with dimensions close to real ZNC nano-particles to obtain accurate energetics and to evaluate interactions in ternary systems.

5.1.2 Formation of prototypical ternary systems

The first step in our investigation concerned the co-adsorption energy of $TiCl_4$ and an ID on the same $MgCl_2$ clusters. Both experimental and computational data suggest that these two species are adsorbed in close proximity on lateral terminations of the support.[3a, 4] On the other hand, these studies didn't report a clear comparison between different co-adsorption models. To assess which is the preferred environment of Ti in a heterogeneous pre-catalyst, we combined the three binding modes of $TiCl_4$ on $MgCl_2$(110) (reported in literature as Corradini,[5] Parrinello[6] and Edge[7] models, see **§ 4.1**) with various binding arrangements of an archetypical donor molecule on the same lateral termination, generating a

plethora of different ternary systems. Due to the large amount of CPU-time needed for these calculations, we focused our efforts by considering only one donor molecule (2,2-dimethyl-1,3-dimethoxypropane, DMMP) and one 'ideal' $MgCl_2$(110)-like cluster of rather modest dimensions (i.e. Clu_110_27, see section 2.2.3).

We evaluated the co-adsorption energy of $TiCl_4$ and donor on the same edge of the cluster, according to the following chemical reaction:

$$TiCl_4 + ID + Clu\_110\_27 \rightleftharpoons Clu\_110\_27/ID/TiCl_4 \qquad \textbf{Eq. 5.1}$$

where the three reagents are considered as independent molecules that are joined together in order to form a ternary system.

The results indicate that the most stable ternary system features an epitaxial $TiCl_4$ chemisorbed next to a chelated donor (see **Figure 5.1-A**). Also for several other structures, ΔG_{ads} values turned out to be strongly negative (-15 ÷ -20 kcal/mol), but they turned out to be far less stable than the previous one (see **Chart 5.1** for a comparison).

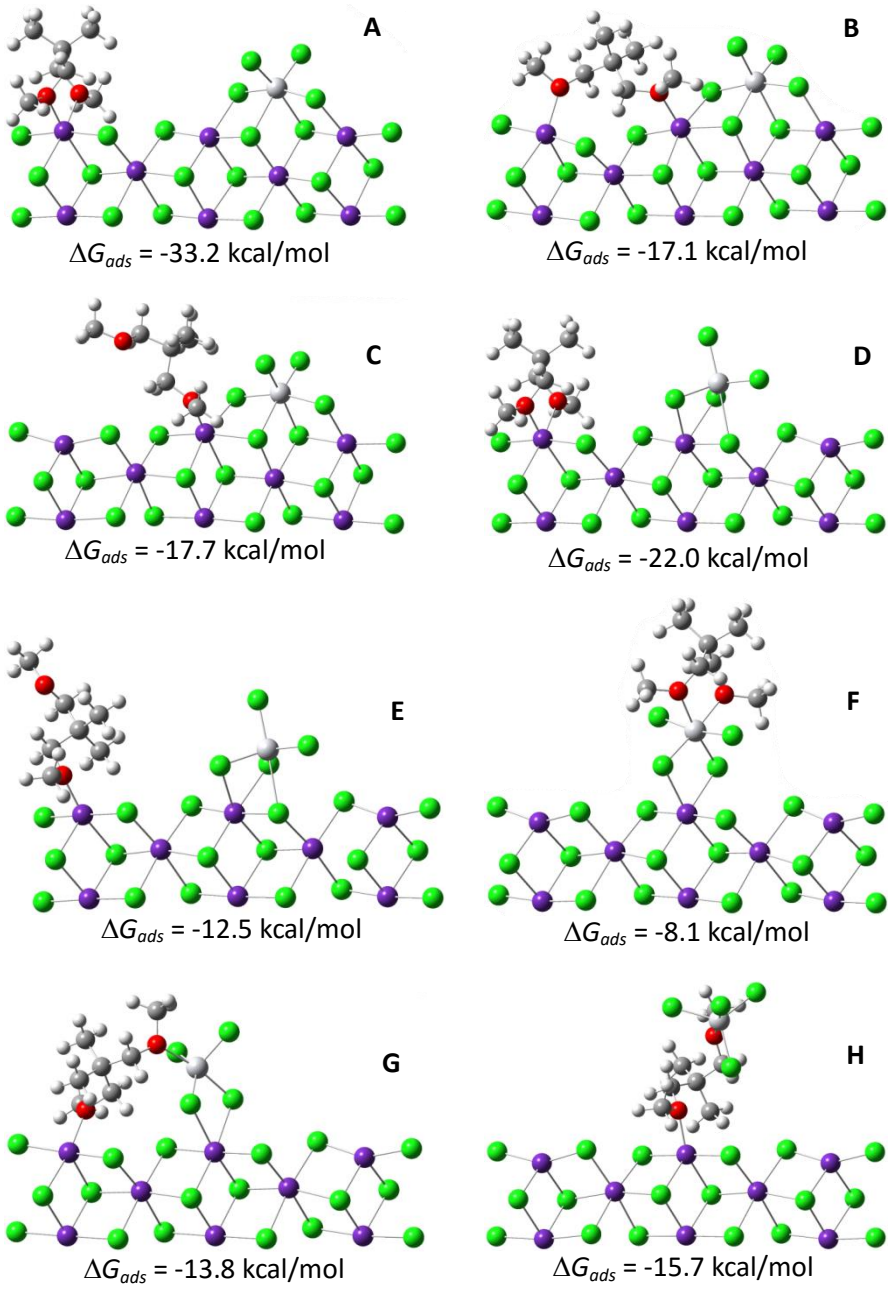

Figure 5.1 Most stable ternary models using DMMP as ID. Corresponding ΔG_{ads} are calculated using **Eq. 5.1**.

Chart 5.1 Relative co-adsorption energies calculated using **Eq. 5.1**. Refer to **Figure 5.1** for a visual representation of the ternary models.

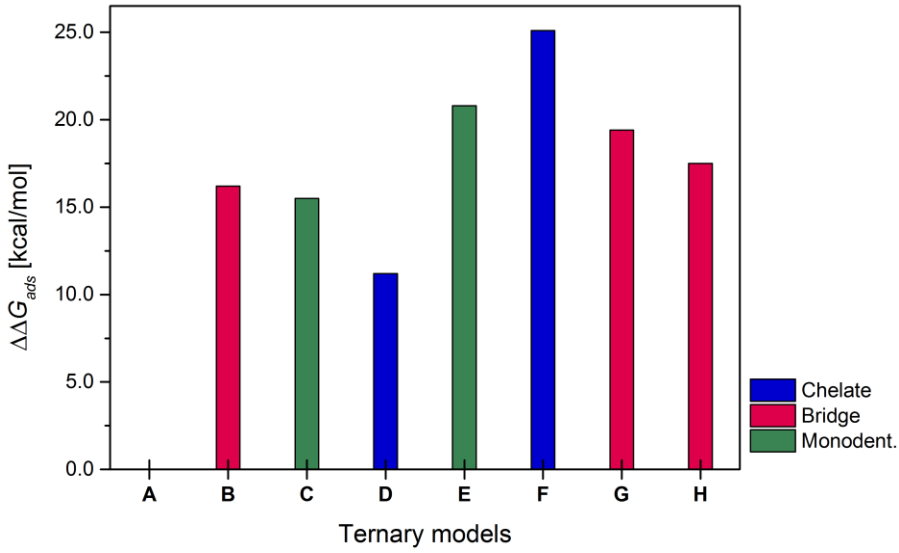

As already mentioned in section 1.2.2, titanation is the final and crucial step during the synthesis of a typical ZNC precursor. The final Ti/donor ratio will strongly influence the steric and electronic environment around each active site. Typically, a large excess of $TiCl_4$ (relative to both $MgCl_2$ and ID) is employed in this reaction with a double purpose:

a) purge $MgCl_2$ nano-particles of all poisoning molecules adsorbed during previous treatments (like H_2O or EtOH);

b) compensate for its much lower affinity for $MgCl_2$ compared to internal donors.

This means that at the start of titanation, the ID is not present as such but rather bound to $TiCl_4$. In order to investigate whether this could have an impact on the kinetics and energetics of adsorption on $MgCl_2$, the

interaction energies of $TiCl_4$ with a number of donor molecules were calculated (**Table 5.1**). The results demonstrate that in most cases complexation is marginally favorable, with Gibbs free energies of formation in the range of -5 ÷ +5 kcal/mol. This means that the presence of $TiCl_4$/donor adducts will have very little influence on the outcome of the titanation, and we can safely ignore formation of such adducts.

$$TiCl_4 + \text{donor} \rightleftharpoons TiCl_4/\text{donor} \qquad \textbf{Eq. 5.2}$$

Table 5.1 Enthalpy, entropy and Gibbs free energy of formation for $TiCl_4$/donor complexes calculated using **Eq. 5.2**. Experimental data in parentheses.

Entry	Structure	ΔH_{ads} [kcal/mol]	$-T\Delta S_{ads}$ [kcal/mol]	ΔG_{ads} [kcal/mol]
1	$TiCl_4$ / DMP[a]	-11.8 (-20.5)	+11.9 (+14.4)	+0.1 (-6.1)
2	$TiCl_4$ / DMP[b,c]	-16.1	+14.6	-1.5
3	$TiCl_4$ / DMP[b,c]	-16.3	+14.4	-1.9
4	$TiCl_4$ / DMSuc[a]	-12.8 (-20.4)	+11.6 (+13.9)	-1.2 (-6.8)
5	$TiCl_4$ / DMSuc[b]	-18.0	+13.9	-4.1
6	$TiCl_4$ / DMMP[a]	-8.3 (-22.9)	+12.8	+4.5
7	$TiCl_4$ / DMMP[b]	-17.5	+14.9	-2.6
8	$TiCl_4$ / DMMSi[a]	-10.3	+13.6	+3.3
9	$TiCl_4$ / DMMSi[b]	-17.1	+15.0	-2.1

[a] Ti with tbp coordination geometry; [b] Ti with octahedral coordination geometry; [c] different donor conformations. Level of theory: M06-2X/(m)aug-cc-pVTZ//RI-TPSS/def2-SVP

In conclusion, our results clearly point to the model of **Figure 5.1-A** as the thermodynamically most stable structure. Thus, this ternary system should be considered as a reasonable starting point for the elaboration of new active site models of realistic size.

5.2 The High-Coverage Model for ZNC active sites

5.2.1 Ti centers in a highly crowded environment

As mentioned in section 2.1.3, typical ZNC nano-particles have dimensions of 4 ÷ 8 nm along the basal plane. Monolayered clusters of this size, with hexagonal shape, have been proposed in literature.[8] Using these structures, we can estimate that the amount of exposed (unsaturated) Mg atoms should be less than 40% of total Mg. Common industrial ZNC contain, in mol% relative to total Mg, about 5 ÷ 10% of Ti species, ~10% of donor molecules, and after activation also ~10% of Al compounds.[9] This leads to the conclusion that the exposed surfaces of $MgCl_2$ primary particles are highly crowded.

A closer inspection of the most stable ternary model, **Figure 5.1-A**, reveals the presence of residual surface vacancies. Indeed, the Van der Waals surface of this model clearly shows single Mg unsaturations next to the $TiCl_4$ adsorption site (**Figure 5.2**). In view of the high degree of coverage observed experimentally, it is possible that such vacancies would be occupied by further donors adsorbed in atypical binding modes (e.g., monodentate instead of bidentate).

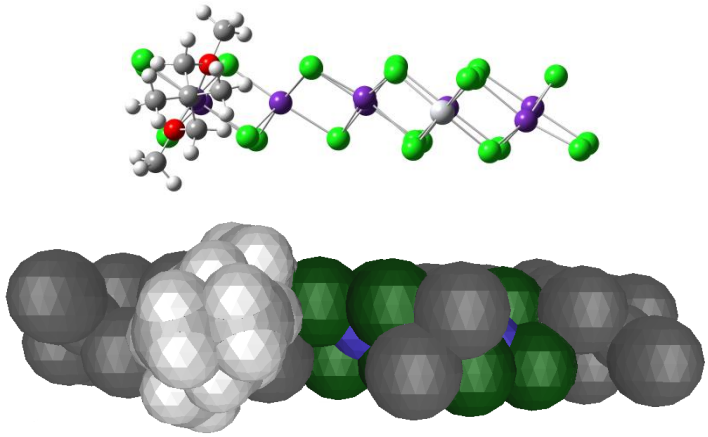

Figure 5.2 Side view of the most stable ternary system and relative Van der Waals surface. Only unsaturated Mg vacancies are colored.

To explore this hypothesis we calculated the binding energy of an extra molecule added to the system of **Figure 5.1-A**; in particular we considered the chemisorption of a second DMMP moiety, as well as that of dimethyldimethoxysilane (DMMSi), in monodentate fashion (**Figure 5.3**). All calculated structures show favorable binding, with ΔG_{ads} for the additional donor varying between -4 ÷ -11 kcal/mol. Of course, sterically demanding substituents can limit chemisorption at these vacant positions, but even having the extremely bulky 9,9-bis(methoxymethyl)-9H-fluorene (BMMF) ID as a neighbor does not prevent DMMSi from monodentate binding in this position (see **Figure 5.3-D**).

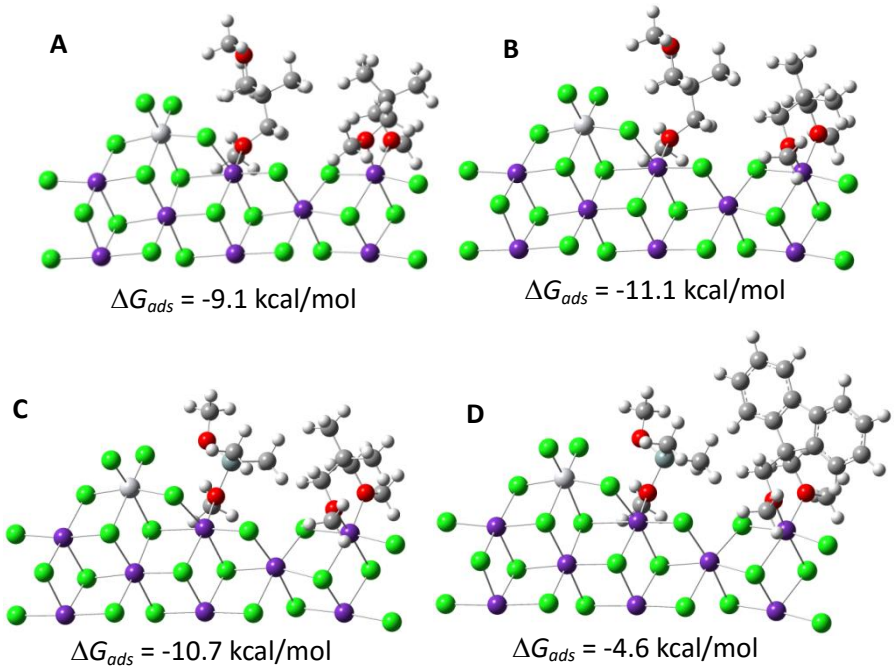

Figure 5.3 Comparison between monodentate DMMP and DMMSi binding to pre-formed ternary system: **A** and **B,** $TiCl_4/\kappa^1$-DMMP/κ^2-DMMP; **C,** $TiCl_4/\kappa^1$-DMMSi/κ^2-DMMP; **D,** $TiCl_4/\kappa^1$-DMMSi/κ^2-BMMF.

We will call these models, which are based on 'classical' ZNC models with the addition of a LB in non-traditional binding mode, "High-Coverage Models". Our results suggest that such models may represent reasonable precursors of catalytic species. They combine a fairly high binding energy with a steric demand at the Ti centers, large enough to result into a regio- and stereoselectivity of propene insertion into a Ti-alkyl bond.

5.2.2 The High-Coverage Model applied to real size systems

Based on the results shown in sections 5.1.2 and 5.2.1, we compared the stereoselectivity of models shown in **Figure 5.4**. These structures feature two chelated DMMP located in close proximity of a Ti(III) center. The neighboring isolated Mg vacancies were left empty in one model (**Figure 5.4-A**, a 'classical' ZNC polymerization site),[9-10] and filled by two monodentate DMMSi molecules in the other model (**Figure 5.4-B**); this allows validation of both the computational approach and the site design. Approximate transition states for primary *re* and *si* propene insertion into the Ti–^{i}Bu bond were located. The energy difference between these two transition states, $\Delta E^{\ddagger}_{Stereo}$, is a measure of the stereoselectivity of these active sites. See **Appendix V** for computational details of the transition states searches.

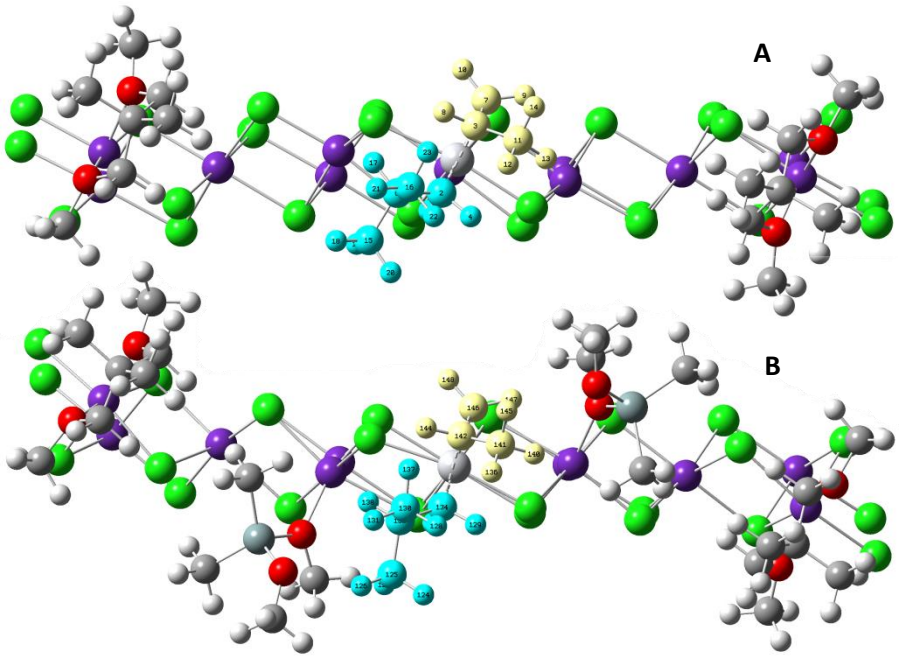

Figure 5.4 Approximate transition state higher in energy for active site systems adopted in this study (**A** = 'classical' ZNC site, **B** = structure of the High-Coverage Model). Monomer is colored n yellow, polymer chain in light blue.

In good agreement with the previous literature, active site models that don't feature any donor coordinated close to the titanium center show poor stereoselectivity (**Table 5.2**). In fact, even the presence of a sterically demanding 1,3-diether (e.g. BMMF) results in a non-stereoselective site. Introduction of external donors in the monodentate positions changes the scenario, turning the site into a stereospecific one.

Table 5.2 Evaluation of the stereoselectivity of the active site models proposed.

Entry	IDs	$\Delta H^{\ddagger}_{Stereo}$ [kcal/mol]	$\Delta G^{\ddagger}_{Stereo}$ [kcal/mol]
1	2DMMP	-0.1	+0.1
2	2BMMF	-0.6	-0.5
3	2DMMP + 2DMMSi	+4.7	+4.4

Level of theory of the calculations: RI-TPSS-D2/def2-TZVPP//RI-BP86/def2-SVP.

This study represents only a preliminary exploration of the potential of both the High-Coverage Model and the Cluster DFT-D Modelling Approach. Indeed, a more comprehensive exploration of ID and ED orientations is required, as well as the evaluation of different cluster models (e.g. defective systems proposed in section 4.2.2) in order to provide an extensive and exhaustive representation of the main plausible ZNC active sites.

Reference

1. (a) Corradini, P.; Guerra, G.; Cavallo, L., *Acc. Chem. Res.* **2004,** *37* (4), 231-241; (b) Cavallo, L.; Guerra, G.; Corradini, P., *J. Am. Chem. Soc.* **1998,** *120* (10), 2428-2436; (c) Seth, M.; Ziegler, T. In *DFT-QM/MM examination of possible active sites in TiCl4/MgCl2 based heterogeneous Ziegler-Natta catalysts*, American Chemical Society: 2001; pp INOR-433; (d) Seth, M.; Margl, P. M.; Ziegler, T., *Macromolecules* **2002,** *35* (20), 7815-7829.
2. (a) Vanka, K.; Singh, G.; Iyer, D.; Gupta, V. K., *J. Phys. Chem. C* **2010,** *114* (37), 15771-15781; (b) Taniike, T.; Terano, M., *J. Catal.* **2012,** *293* (0), 39-50; (c) Stukalov, D. V.; Zakharov, V. A., *J. Phys. Chem. C* **2009,** *113* (51), 21376-21382; (d) Stukalov, D. V.; Zilberberg, I. L.; Zakharov, V. A., *Macromolecules* **2009,** *42* (21), 8165-8171; (e) Correa, A.; Piemontesi, F.; Morini, G.; Cavallo, L., *Macromolecules* **2007,** *40* (25), 9181-9189.
3. (a) Bazhenov, A. S.; Denifl, P.; Leinonen, T.; Pakkanen, A.; Linnolahti, M.; Pakkanen, T. A., *J. Phys. Chem. C* **2014,** *118* (48), 27878-27883; (b) Correa, A.; Credendino, R.; Pater, J. T. M.; Morini, G.; Cavallo, L., *Macromolecules* **2012,** *45* (9), 3695-3701; (c) Kumawat, J.; Kumar Gupta, V.; Vanka, K., *Eur. J. Inorg. Chem.* **2014,** *2014* (29), 5063-5076; (d) Credendino, R.; Liguori, D.; Fan, Z.; Morini, G.; Cavallo, L., *ACS Catalysis* **2015,** *5* (9), 5431-5435.
4. (a) Liu, B.; Nitta, T.; Nakatani, H.; Terano, M., *Macromol. Chem. Phys.* **2003,** *204* (3), 395-402; (b) Busico, V.; Cipullo, R.; Monaco, G.; Talarico, G.; Vacatello, M.; Chadwick, J. C.; Segre, A. L.; Sudmeijer, O., *Macromolecules* **1999,** *32* (13), 4173-4182.
5. Corradini, P.; Barone, V.; Fusco, R.; Guerra, G., *Gazz. Chim. Ital.* **1983,** *113* (9-10), 601-7.
6. Boero, M.; Parrinello, M.; Terakura, K., *J. Am. Chem. Soc.* **1998,** *120* (12), 2746-2752.
7. Monaco, G.; Toto, M.; Guerra, G.; Corradini, P.; Cavallo, L., *Macromolecules* **2000,** *33* (24), 8953-8962.
8. Credendino, R.; Pater, J. T. M.; Correa, A.; Morini, G.; Cavallo, L., *J. Phys. Chem. C* **2011,** *115* (27), 13322-13328.
9. Moore, E. P., Jr., Ed., *Polypropylene Handbook: Polymerization, Characterization, Properties, Processing, Applications*. Hanser Publishers:

Munich, Germany: 1996.
10. Lee, J. W.; Jo, W. H., *J. Organomet. Chem.* **2009,** *694* (19), 3076-3083.

Chapter 6. Conclusions and general remarks

This dissertation focused on Quantum Mechanical simulation of heterogeneous Ziegler-Natta Catalysts (ZNCs) for the industrial production of isotactic polypropylene. Despite the fact that this material is the second largest volume synthetic polymer worldwide, both industry and academia seem to be reducing their investments in research addressing fundamental questions about ZNCs.

In **Chapter 1**, we reported a brief historical overview explaining the serendipitous choice of supporting chiral Ti-based active species onto a nano-crystalline $MgCl_2$ matrix. The addition of organic surface modifiers (Lewis bases, called internal and external donors in this context) strongly improves regio- and stereoselectivity of the catalytically active centers, leading to the production of astonishingly regular polymers. Tentative explanations of this behavior have been based on many different experimental observations, but the extreme reactivity and heterogeneous nature of the catalysts often complicates interpretation of observations.

A theoretical approach to this problem in principle allows careful evaluation of the contributions of each individual catalyst component to the overall predicted behavior. This argument is based on the assumption that present-day computational tools are capable of a 'comprehensive description' of the system of interest. The 'description' of ZNCs has evolved over time with the development of more accurate and reliable

computational methods, and will most likely keep on evolving. This implies that theories based primarily on computational results have to be periodically verified and, sometimes, revisited. In the present thesis, we attempt to develop a systematic "from the ground up" approach to the modelling of ZNC. We do not promote one specific model, but instead concentrate on methodology to reliably asses possible models.

The Cluster DFT-D Modelling Approach reported in **Chapter 2** was developed on the basis of experimental evidence and the use of state-of-the-art of the Density Functional Theory (DFT) methods. A meticulous validation of the computational protocol (designed to handle hundreds of atoms at a time) provides the confidence that we can freely produce and evaluate new models; we have also identified a few areas of concern.

With this in mind, in **Chapters 3** and **4** we apply this approach to the adsorption of industrially relevant Lewis base molecules and of $TiCl_4$ (the most common precursor of catalytic centers) on unsaturated surfaces of $MgCl_2$. Our results essentially confirm qualitative findings already claimed in recent literature. They nevertheless represent a significant step forward because the evaluation of thermochemical corrections makes the model more quantitative and provides more data for comparison with experiments.

In **Chapter 5**, these models are then combined to explore the formation of many different ternary systems, as potential models for realistic ZNC precursors. Intriguingly, the thermodynamically most stable ternary system we studied resembles one of the ‘classical’ Corradini models

(featuring an epitaxial $TiCl_4$ adsorbed next to a chelating 1,3-diether), but one that according to Corradini - and to our own calculations - would *not* be isospecific! However, a consideration of primary particle size and the amounts of catalyst components in real ZNCs reveals that this model is probably not realistic. Instead, we propose a "High-Coverage Model" that *starts* with Corradini's aselective site but makes it selective through binding of additional donors in a less traditional fashion. Our first tests of this model appear to be in good agreement with common experimental observations.

This leads to the conclusion of our dissertation, in which we not only arrive at new and more detailed answers about the nature of ZNCs, but also at a new computational protocol specifically designed to study heterogeneous systems with a high degree of accuracy.

This work is part of the research program of the Dutch Polymer Institute (DPI), Project #754.

As of 31st March 2016, clearance by the DPI Program Committee is pending. Amendments to the present text might be requested until the date of publication.

Appendix I. Quantitative determination of H_2O in $MgCl_2$ samples

This analysis involves a Pyrex bottle of 70 mL with a perforated SVL screw top in which will be located a silicon septum. After a night at 135°C, the equipment is transferred inside a glove-box LabMaster 130 with an Ar atmosphere to load ~1.0g of $MgCl_2$. Then the bottle is closed and 20.0 mL of a 6.0M solution of trimethylaluminum (TMA, Chemptura) in anhydrous heptane (HPLC-grade, further purified using an MBraun mod. SPS-5 system) are added using a polyethylene syringe. After 20 minutes of vigorous stirring, 0.2 mL of the gas phase is injected in a gas chromatograph Carlo Erba Vega 6000 (equipped with an packed column of 2 meters and FID detector) to determine the amount of CH_4 obtained by the hydrolysis of TMA. We assumed that 2 mol of CH_4 were formed per mol of H_2O.

The same operations are repeated for a blank experiment and the H_2O content of the $MgCl_2$ sample is calculated from the difference between the two experiments.

Table I.1 Amount of CH_4 measured via gas chromatography.

System	CH_4 [mL]	n (H_2O)/n (Mg) [%]
'anhydrous' $MgCl_2$	5.7	1.7
blank	0.7	

Appendix II. Dehydration of $MgCl_2$ samples

Operating inside a glove-box, 10 ÷ 15 g of $MgCl_2$ and 80 mL of anhydrous heptane (see **Appendix I** for details) are introduced in a Pyrex reactor equipped with a siphon and a sintered-glass filter (see **Figure II.1-A**). The reactor is connected to a Schlenk line (see **Figure II.1-B**). Under an abundant flow of argon, 40 mL of $SiCl_4$ (Fluka, purity >99%) are introduced. The reactor is kept 55 ÷ 65°C in an oil bath for 5 hours. During this operation, a slow flow of Ar is maintained in order to protect the system and to flush HCl from the gas phase.

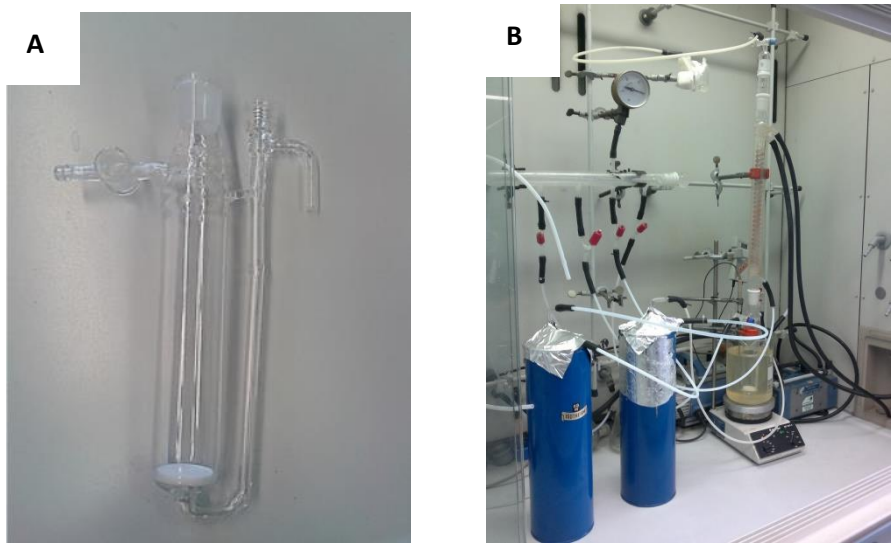

Figure II.1 Reactor in Pyrex used for the dehydration of $MgCl_2$ (**A**) and the apparatus connected to a Schlenk line (**B**). All the components of this apparatus were treated at 135”C overnight.

After this operation, the liquid phase is collected in a cold trap (cooled with liquid N_2) via the siphon. The solid phase collected on the glass frit is dried for 30 minutes at >100°C under vacuum. Then 100mL of anhydrous heptane are added to wash the solid phase at 70°C for 30 minutes. Next, the liquid phase is removed and the solid phase is dried again for 30 minutes at >100°C under vacuum. A final washing is carried out with 100mL of pentane at room temperature for 30 minutes and then the solid phase is dried overnight at >100°C under vacuum. The sample is stored inside a glove-box with an inert atmosphere of Ar (concentration of H_2O and O_2 below 1 ppmv).

Appendix III. Milling of $MgCl_2$ and $MgCl_2$/ID samples

To prepare our milling samples, we used a planetary ball mill (Retsch model PM 100, see **Figure III.1**) equipped with an air-tight 50 mL jar made of ZrO_2 stabilized with Y (treated at 100°C under vacuum overnight). Inside a glove-box, the jar is loaded with 3 ÷ 5 g of $MgCl_2$ and ~50 g of ZrO_2 spheres with a diameter of 3 mm (also treated at 100°C under vacuum overnight). If donors are used (e.g. DMMP and DIBP) they are also added at this stage, see section 2.1.3. The jar is closed and inserted in the mill. The mill was programmed to run at 650 rpm for 8 hours, divided in 20-minute periods interrupted by 5-second breaks to allow the motor of the mill to invert the direction of rotation; this protocol was found to result in a more homogeneous material.

Figure III.1 Planetary ball mill Retsch mod. PM 100.

At the end of the milling process, the sample is collected in a glove-box. In case of $MgCl_2$/ID systems, the powder is recovered with 30 mL of heptane and transferred inside the reactor of **Figure II.1-A** for washing as described in **Appendix II**.

Powder XRD spectra were collected using a Philips diffractometer PW 1830 with a custom-designed air-tight cell (see **Figure III.2**). Diffraction profiles were collected using Ni-filtered CuKα radiation (30 mA, 35 KV), with a step scan procedure (from 2θ 5.0 to 70.0° in steps of 0.1°; 20 seconds of signal collection).

Figure III.2 Custom-designed air-tight X-ray cell adopted in this study.

Appendix IV. Adsorption of donor molecules on preformed $MgCl_2$

This study is conducted inside a triple glove-box MBraun Lab Master in an atmosphere of N_2 equipped with a Symyx (now Freeslate) Extended Core Module (see **Figure IV.1**). This platform has two robotic arms to dispense solid, liquid and suspensions, two decks for reaction at variable temperatures with magnetic stirring, one deck for mechanical stirring and an analytic balance Sartorius WZ614-CW with ion-suppressor system. In the same glove-box is also located an internal centrifugal drying station Savant SPD121P.

Figure IV.1 View of the Symyx Extended Core Module.

For our experiments we used a matrix of 24 8 mL Pyrex vials with screw caps. 25 mg of pre-milled $MgCl_2$ and an adequate volume of a solution of donor in heptane (for a total volume of 3.5 mL) are loaded in each vial, and then the suspensions are stirred (800 rpm) at 70°C for one

hour. The vials are rapidly cooled in a freezer at -17°C to quench the adsorption reaction. Following, the matrix is centrifuged per 10 minutes at 800 rpm and the liquid phase is removed. The solid phase is washed using the procedure described in **Appendix II** (2.5 mL of solvent per vial). Finally, the solid phase is dried under vacuum at 45°C in the centrifugal station for one night.

The amount of donor adsorbed is determined by ^{1}H-NMR (Bruker Avance DRX 400 operating at 400MHz), after dissolution of the solid phase in deuterated methanol with acetonitrile as internal standard.

Appendix V. Computational details of transition states searches

Due to an unexpected difficulty in optimization of the structures examined, we slightly modified the calculation protocol reported in section 2.2.1, adopting the BP86 functional (defined in Turbomole as a Slater-Dirac LDA + Becke 88 functionals for the exchange part and Vosko-Wilk-Nusair + Perdew 86 functionals for the correlation part)[1] for geometry optimization. Also in this case, RI and MARI-J accelerator were adopted. Instead of performing a full transition state search, the new C-C bond between the monomer and the polymer chain was fixed at 2.1 Å, in agreement with 'classical' ZNC models.[2]

Frequency analysis (carried out at RI-BP86/def2-SVP level of theory) reveals the presence of only one imaginary frequency, corresponding to the reaction coordinate investigated.

Further evaluation of the electronic energy of said optimized structures was conducted as for all other structures studied in this thesis (i.e. single point calculation at RI-TPSS-D2/def2-TZVPP level of theory).

Reference

1 a) Dirac, P. A. M., *Quantum Mechanics of Many-Electron Systems*, **1929**; Vol. *123*, p 714-733; b) Slater, J. C., *Phys. Rev.* **1951**, *81*, 385-390; c) Becke, A. D., *Phys. Rev. A* **1988**, *38*, 3098-3100; d) Vosko, S. H.; Wilk, L.; Nusair, M., *Can. J. Phys.* **1980**, *58*, 1200-1211; e) Perdew, J. P., *Phys. Rev. B* **1986**, *33*, 8822-8824.

2 Cavallo, L.; Guerra, G.; Corradini, P., *J. Am. Chem. Soc.* **1998**, *120*, 2428-2436.

Acknowledgments

First of all, I'd like to thank Prof. Vincenzo Busico that gave me the opportunity to carry out this PhD project in his group and guide me into my scientific growth with great passion and competence. Moreover, he had also the laborious duty of translating many of my craziest ideas in scientific discoveries.

I am also extremely grateful to Prof. Peter Budzelaar that helped me to move the first steps in those marvelous worlds of computational science and of computer managing… both joy and pain of the last three years and for the rest of my life…

A special thank-you also to Prof. Roberta Cipullo, for the numerous NMR analyses; they were essential to carry out my project.

Many thanks to Prof. Luigi Cavallo that gave me the opportunity to spend a few months in his research group at the King Abdullah University of Science and Technology.

I am also grateful to Dr. Christian Ehm for the infinite discussions about science and life (usually in presence of beers and burgers)… I will always have a "but" for you and an ear too small to hear your answer!!!

Thanks also to Dr. Andrea Correa who taught me how to write a scientific article and how to deal with a supercomputer center.

I like to thank all the people that were directly (or indirectly) involved in the realization of this project. First of all, all the members of LSP

Research Group and HTExplore: Alessio, Enrichetta, Alessia, Pasquale, Marina, Giuseppe, Francesco, Antonio and Eric (from time to time). Then, the students that shared with me the room 2p-15, in particular Chiara, Salvatore, Vittoria, Selene, Domenico, Andrea, Fiorella, Alessio, Stefania, Raffaele and Miriana. All of you helped me to combine an austere scientific research with funnier moments… and to provide an infinite number of broken computers for my Saturday morning!!!

I also need to thank my friends, and in particular David and Bianca for the Scientific Coffee of 8.30; Umberto for sharing his own personal experience with servers and software; Stefania, Flo, Laura, Luca, Corrado, Emanuele, Eva, Sergei, Theo, Julien, Yuri, Edrisse, Sai and Abdou for the hundreds of pleasant moments I had at KAUST.

Finally, a special thank-you to my family that allows me to stay away from home for such a long time in spite of all the difficulties that they had to face (especially in the last period). They always reserved for me a smile and a comfortable bed, asking only for some black cherry biscuits and few Neapolitan sandwiches.